

# Entanglement structure of current driven quantum many-body systems

Michael J. Gullans<sup>1</sup> and David A. Huse<sup>1</sup>

<sup>1</sup>*Department of Physics, Princeton University, Princeton, New Jersey 08544, USA*

(Dated: July 21, 2022)

When an extended system is coupled at its opposite boundaries to two reservoirs at different temperatures or chemical potentials, it cannot achieve a global thermal equilibrium and is instead driven to a set of current carrying non-equilibrium states. Motivated by developments in the understanding of thermalization in closed quantum many-body systems, we find conditions under which such current-driven systems can achieve, or violate, local thermal equilibrium by investigating their entropy, mutual information, and entanglement at long times. We focus on a specific model consisting of a two-parameter family of random unitary circuits acting locally on a chain of spin-1/2s (equivalently, qubits) that exhibits quantum chaotic behavior in most of its parameter space. The only conserved quantity is the total magnetization of the spins. We choose the model so that for all parameter values the time-averaged correlation functions agree and are close to local equilibrium. However, computing the total von Neumann entropy of the system shows that there are in fact three distinct “phases” of the driven problem, with local equilibrium only emerging in the quantum chaotic regime, while one of the other phases exhibits volume-law mutual information and entanglement. We extend these results to the three-dimensional, non-interacting Anderson model in the diffusive regime, showing that the non-equilibrium steady-state for fermions realizes the volume-law mutual information phase of the random circuit. Our results suggest a generic picture for the emergence of local equilibrium in current-driven quantum chaotic systems, as well as provide insights into methods to stabilize highly-entangled many-body states out of equilibrium.

## I. INTRODUCTION

Uncovering general principles that describe the entanglement structure of quantum many-body systems is a fundamental challenge in statistical mechanics and quantum information science [1]. In the ground state of local Hamiltonian systems, the entanglement entropy often satisfies an area law, whereby the entropy of a sub-region scales with the area of its boundary [2–5]. At thermal equilibrium at nonzero temperature, this scaling becomes a volume law for pure states [6–8], but the mutual information of equilibrium thermal *mixed* states still exhibits an area law [4]. The existence of such area laws allows a rich set of analytical and numerical tensor network techniques to be used to characterize and classify these states [9–11]. Although area laws are typical of thermal mixed states, any modification that drives the system out of equilibrium allows for potential violations.

A standard non-equilibrium scenario consists of a system coupled to two reservoirs with different chemical potentials, which drives currents in the system. The analog of thermalization in these systems is the approach to local equilibrium at long times, which is often assumed when describing the transport properties of strongly interacting, quantum chaotic systems [12–15]. For classical versions of this problem, a large body of work has been devoted to deriving emergent hydrodynamic descriptions of hard-core stochastic lattice gases [16, 17]. In this case, rigorous arguments have been formulated showing that the entropy for a large class of these models converge to local equilibrium (up to sub-volume corrections) [18, 19]. At the same time, it has been found that, even in one dimension, these boundary driven classical systems exhibit behavior traditionally associated with critical models at

equilibrium, such as power-law correlations and spontaneous symmetry breaking [20–23], making them a rich avenue for investigation. Studies of quantum versions of these current-driven problems have mainly focused on integrable or free-fermion models [24–31]. Provided the system is not in a many-body localized phase, adding integrability breaking terms or interactions to these models generally leads to diffusive dynamics at long times [32–36]. Other work has aimed at finding efficient tensor network descriptions of the steady states of these models based on the assumption that they satisfy an area law or have an integrable structure [37–41]. A related quench problem considers two identical many-body systems at different temperatures or chemical potentials suddenly brought into contact and allowed to evolve. For integrable models the steady-state for this problem is typically non-thermal [42–44], which has been shown to lead to a logarithmic violation of the area law for the mutual information [45] and entanglement [46–49].

To determine more general conditions under which the steady-state of current-driven models achieve or violate local equilibrium, here we investigate a two-parameter family of such models with a strongly interacting regime that exhibits quantum chaotic behavior. The model also shows two other distinct “phases” of non-chaotic behavior at certain limiting (thus “fine-tuned”) values of its parameters. Our system is a spin-1/2 chain with the magnetization of the spins being the “charge” that is conserved and that is being transported by the current. Away from the boundaries the dynamics is unitary, and is given by a random quantum circuit with gates acting locally on the spins; this allows us to obtain many results analytically. At long times each specific realization of this boundary-driven system converges, for all initial condi-

tions, to a particular time-dependent mixed state that we call a “non-equilibrium attracting state” (NEAS) in analogy to the nomenclature of a non-equilibrium steady-state (NESS) for driven time-independent systems. The time-averaged correlation functions and current are the same for all parameters in this model and, up to small corrections, can be computed from local equilibrium.

Despite this uniform time-averaged behavior, we find three different phases for the instantaneous NEAS when we look at its von Neumann entropy, mutual information, and entanglement properties. The generic behavior is quantum chaotic and is, as one might expect, close to local thermal equilibrium. For certain limiting values of the parameters of the model, we obtain two other fine-tuned phases whose entropy deviates extensively from local equilibrium, one of which also exhibits volume law mutual information and entanglement (as measured by the logarithmic negativity) of its instantaneous NEAS many-body density matrix. Although we derive these results for a specific one-dimensional random circuit model, some of the qualitative behavior is more general and should apply to more “physical” situations in higher dimensions and with time-independent Hamiltonians. In particular, we show numerically that the volume-law mutual information phase is realized for fermions in the diffusive regime of the three-dimensional (3D) non-interacting Anderson model. Surprisingly, given the long history of that subject, the presence of such a volume-law mutual information in the NESS of the driven 3D Anderson model has not been previously uncovered to our knowledge.

## II. EMERGENCE AND VIOLATION OF LOCAL EQUILIBRIUM

The general setup we consider is shown in Fig. 1(a) and consists of a system with a global conservation law (either magnetization or particle number) in contact with two thermodynamic reservoirs at different chemical potentials. The chemical potential bias leads to steady-state currents in the long time limit. The models we consider have an effective hydrodynamic description for the average value of the conserved quantity  $n(\mathbf{r}, t)$  given by the diffusion equation

$$\frac{\partial}{\partial t} n(\mathbf{r}, t) = \tilde{D} \nabla^2 n(\mathbf{r}, t), \quad (1)$$

where  $\tilde{D}$  is the scaled diffusion constant and  $\mathbf{r}$  is a  $d$ -dimensional position vector scaled so that  $x = 0/1$  corresponds to the longitudinal position of the left/right reservoir. When subject to the boundary condition  $n(\mathbf{r})|_{x=0} = n_L$  and  $n(\mathbf{r})|_{x=1} = n_R$ , this equation has the steady-state solution shown in Fig. 1(b)

$$n(\mathbf{r}) = n_L(1 - x) + n_R x. \quad (2)$$

This average profile, however, gives limited information about the entanglement structure of the steady-states,

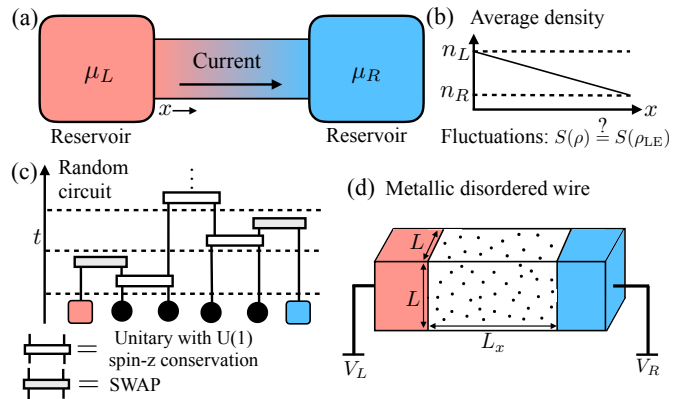


FIG. 1: (a) Current driven model we consider where two reservoirs are held at fixed chemical potentials and the bulk dynamics conserves the total density. (b) The average local density will generically be linear in the position, but the total von Neumann entropy may have an extensive (“volume-law”) deviation from local equilibrium. (c) We focus on a random circuit model for the bulk dynamics, which exhibits quantum chaotic behavior for some parameter regimes. The interaction with reservoir is accounted for by a SWAP gate that acts immediately after any other gate is applied to the boundary spin. (d) We also consider the metallic regime of non-interacting fermions in a disordered 3D wire and find they display a similar volume law entanglement structure as one of the phases of the random circuit.

which is generically encoded in high-degree correlation functions. To investigate the entropy and entanglement properties of such current driven quantum systems more systematically we analyze the two models shown in Fig. 1(c-d). Due to its simple structure and analytic tractability, we focus on a random circuit model with charge conservation in most of this paper. Indeed, for this reason, similar random circuit models have been widely used to investigate dynamics in quantum chaotic systems [50–60]. As there is no energy conservation for the random circuit, local equilibrium is simply defined as the product state density matrix with the same average magnetization profile as (2). One distinction between the Anderson model and the random circuit is that the Anderson model is also subject to energy conservation. In fact, it is known from theoretical studies [61–63] and experimental measurements [64] that the local energy distribution function of diffusive non-interacting wires strongly deviates from local equilibrium. Thus the question we address in the context of the Anderson model is how the entanglement structure for the NESS density matrix within a single disorder realization compares to the disorder-averaged density matrix.

### A. Local random circuit with charge conservation

Before describing our results in detail, we first give an “informal” general picture for the entanglement structure and the emergence or not of local equilibrium in the random circuit model. As mentioned in the introduction, we find three phases primarily distinguished by the presence or absence of quantum chaotic behavior. To tune between these three phases we draw the nearest-neighbor random gates according to a two-parameter measure  $d\mu$  over three gate sets  $\mu_{0,1,2}$ :

$$d\mu = (1 - p_1 - p_2)d\mu_0 + p_1d\mu_1 + p_2d\mu_2, \quad (3)$$

where the probabilities  $p_{1,2}$  satisfying  $p_1 + p_2 \leq 1$  are our tuning parameters. To gain some intuitive understanding for the action of the three gate sets on the qubits it turns out to be more convenient to work in a fermion representation of the spins after a Jordan-Wigner transformation. In this representation, the gates in  $\mu_0$  only induce discrete hopping of the fermions between sites, which leads to diffusive transport of the fermion density, (i.e., magnetization), since the position of the gate is also chosen randomly. In  $\mu_1$  we allow “partial swaps” of the qubits, which, in the fermion representation, can break up local fermion density operators  $n_i = c_i^\dagger c_i$  into creation  $c_i^\dagger$  and annihilation  $c_i$  operators that act on different sites, but we forbid gates that induce interactions between the fermions. In  $\mu_2$  the gates are allowed to induce random phases on each state of the fermion occupations, which generates interactions between the fermions, but there are no partial swaps in  $\mu_2$ . These gates allow the operators  $c_i^\dagger$  and  $c_i$  to generate local density operators  $n_i = c_i^\dagger c_i$  by mapping, for example,  $c_i \rightarrow c_i n_{i+1}$ , but they do not break up the local density operators. By combining gates from  $\mu_1$  and  $\mu_2$  one can generate any two-qubit unitary that conserves the total fermion number.

Our motivation for distributing the gates according to (3) is based on the fact that ballistic operator spreading, which is associated with fast scrambling and quantum chaos, only emerges in a two-step process that requires both  $p_1$  and  $p_2$  to be nonzero. The general picture for operator spreading in high-temperature quantum chaotic spin models without a conservation law was developed in Ref. [53–55]. More recently, these results were generalized to the case with a conservation law [56, 57], where it was found that during the evolution induced by the random circuit, an initially non-trivial local operator  $\mathcal{O}_i$  at site  $i$  can generally be decomposed into two components: a conserved component that spreads diffusively with the diffusion constant  $D$ , and a non-conserved component distributed across an exponentially growing number of operator strings each of which has a maximum length and number of non-trivial operators that scales as  $v_B t$ , where  $v_B$  is the butterfly velocity. In the case of the random circuit model considered in this work, we can describe the operator spreading process through coupled equations for the coarse grained density of local density operators  $n_o(x, t)$  and creation  $c(x, t)$  operators at the

low-density “front” of the non-conserved component of the spreading operator

$$\frac{dn_o}{dt} = \tilde{D} \frac{d^2 n_o}{dx^2} - r_1 n_o + 2r_2 c, \quad (4)$$

$$\frac{dc}{dt} = \tilde{D} \frac{d^2 c}{dx^2} + r_1 n_o, \quad (5)$$

where  $r_1 \sim p_1$  and  $r_2 \sim p_2$  are the rates for generating creation and local density operators, respectively. These equations describe a runaway process whereby the non-interacting fermion gates from  $\mu_1$  break up density operators into creation and annihilation operators, which then allows the generation of more density operators through the application of the interaction gates from  $\mu_2$ . The diffusion constant is always order one for these random circuits, but, for small  $p_1$  and  $p_2$ , Eq. (4)-(5) predict the scaling of the butterfly velocity as

$$v_B^2 \sim \min(\sqrt{p_1 p_2}, p_2). \quad (6)$$

The asymmetry between  $p_1$  and  $p_2$  arises from the fact that the partial swaps in  $\mu_1$  only move operators but do not produce new operators, while the interactions in  $\mu_2$  can make new density operators. As a result, for weak interactions,  $p_2 \ll p_1$ , the front is primarily composed of  $c_i$  and  $c_i^\dagger$  with a low density of  $n_i$ , and the faster  $p_1$  process is at local equilibrium even within the front. Thus the front speed is limited only by  $p_2$ . On the other hand, in the opposite regime  $p_1 \ll p_2$ , the front contains primarily  $n_i$  operators and the  $p_1$  process is not at local equilibrium within the front. In this case both processes are important within the front, since one needs to break up the density operators to maintain the locally low density of creation and annihilation operators, which in turn make new density operators. For either  $p_1$  or  $p_2$  equal to zero, the butterfly velocity is exactly zero, which is the origin of the two distinct non-chaotic phases described in the introduction.

We now move to the description of the long-time behavior of the current driven problem with open boundaries. The crucial feature of the quantum chaotic phase for finite  $p_1$  and  $p_2$  (phase III) is the presence of ballistic operator spreading, whereas the operator spreading is diffusive in phases I and II, where  $p_1 = 0$  and  $p_2 = 0$ , respectively. This separation of time scales between the spreading of correlations and the diffusion of the conserved charge leads to a simple heuristic picture for the emergence of local equilibrium. Due to the action of the partial swaps in phases II and III, the system’s non-equilibrium attracting state (NEAS) density matrix is constantly “emitting” non-conserved operators at a rate per site that scales as the square of the current  $J^2 \sim \delta^2/L^2$  (where  $\delta$  is the end-to-end difference of the of the local magnetization, and  $L$  is the length of the system). In phase III, these non-conserved operators spread ballistically at speed  $v_B$  and thus only “live” for a time  $\sim L/v_B$  before they reach a boundary and are “absorbed” (decohered) by that reservoir, implying that

they can only accumulate to a density on the order of  $\delta^2/L$ . Since these non-conserved operators are needed to describe the history of the unitary dynamics in the bulk, when they are quickly lost to the reservoir and remain at a low-density, the deviation  $\Delta S \equiv S(\rho_{\text{LE}}) - S(\rho)$  of the von Neumann entropy  $S(\rho) = -\text{Tr}[\rho \log \rho]$  from the density matrix of local equilibrium  $\rho_{\text{LE}}$  remains small.

Understanding the volume law deviation of the entropy from local equilibrium in the other two phases requires separate consideration: In phase I the argument above no longer applies because the absence of partial swaps implies that the NEAS has zero rate for “emitting” non-conserved operators. In this case, the extensive deviation from local equilibrium is encoded in the single-site spin densities: in the NEAS, each site came most recently from one of the two reservoirs and it still has that spin density. In phase II, the “emission” process is present, but the non-conserved operators spread only diffusively so they build up to a density on the order of  $\delta^2$ . We find that this high density of non-conserved operators leads to a volume law deviation of the entropy, mutual information, and entanglement away from local equilibrium. Here the mutual information between two regions  $A$  and  $B$  is defined in terms of the von Neumann entropy as  $I(A : B) \equiv S(\rho_A) + S(\rho_B) - S(\rho_{AB})$ , where  $\rho_C$  is the reduced density matrix on region  $C$ . To establish the volume law scaling of the entanglement in this phase, we use an entanglement measure known as the logarithmic negativity [65]. Similar to the area law for the mutual information, recently an area law for the logarithmic negativity was proved for thermal mixed states [66], thus, the emergence of phase II is a manifestly non-equilibrium effect.

## B. Non-interacting Anderson model

Our result that phase II exhibits volume-law mutual information and entanglement is rather surprising as such behavior is forbidden in finite-temperature equilibrium systems with local interactions. To explore the general applicability of this finding, we also investigate the NESS (non-equilibrium steady-state) of the 3D disordered Anderson model for non-interacting fermions in the metallic phase (see Fig. 1(d)). Although the arguments presented above seemingly extend in a straightforward manner to this diffusive system, it is helpful to understand how such extensive long-range correlations can emerge using a description that also explicitly takes into account energy conservation.

We model the driven problem by taking a finite region of disordered wire connected at its two ends to ballistic leads that are otherwise identical to the central region. The correlations in the NESS are determined by the properties of the scattering states in a narrow energy range (up to thermal broadening) between the chemical potentials of the two leads. There are two sources of correlations that then give rise to the mutual informa-

tion: First, there is a finite range of energies over which the scattering state wavefunctions are correlated in the disordered region. This energy scale is simply set by the Thouless energy, which is the inverse of the diffusive transit time through the wire  $E_{\text{Th}} = \hbar D/L_x^2$  where  $D$  is the diffusion constant and  $L_x$  is the longitudinal length of the disordered region (assumed to be nearly equal to the transverse width  $L$ ) [67, 68]. Crucial to the existence of the diffusive phase in 3D is that the Thouless energy is much larger than the average level spacing in the wire  $\sim 1/L^2 L_x$  [68]. In the context of the NESS, this scaling implies that the eigenfunctions of the open system are significantly modified due to the coupling to the leads. In addition to these energy correlations, there are correlations between transverse scattering channels that arise because the transport through the wire is not completely ergodic when  $L_x \sim L$ . Accounting for both these types of contributions, we find that we recover the volume-law scaling of the mutual information predicted from the diffusion model for phase II. Note that this effect is absent in equilibrium because the scattering states originating from each lead are then equally populated and interfere with each other to cancel the long-range correlations present in the eigenfunctions. For a ballistic conductor biased at its two ends, a simple calculation shows that there is no similar buildup of a volume law mutual information in the NESS.

To our knowledge the presence of these extensive correlations in the NESS of the non-interacting 3D Anderson model has not been previously discussed in the literature. There is a large body of work studying shot-noise correlations of disordered mesoscopic systems [69–71]; however, the presence of such correlations between spatially separated leads follows directly from current conservation and does not provide direct information about the mutual information or entanglement. For free fermion or Luttinger liquid leads connected by a time varying quantum point contact, there is a coincidental relation between the full counting statistics of the current and growth of entanglement entropy in the leads [72, 73]. These studies, however, considered a spatially zero dimensional region between the leads, finding logarithmic growth of entanglement entropy in the time direction, and did not consider steady-state properties. Other related work has considered the ground state entanglement entropy of random spin chains [74, 75] and wavefunction entanglement in the Anderson model (i.e., entanglement entropy of the system with a single occupied eigenstate) [76], finding a logarithmic scaling with system size in both cases.

## C. Overview of the paper

The paper is organized as follows: In Sec. III we present the random circuit model with charge conservation, analyze the time-averaged behavior and derive the phase diagram for this model. We then show that the NEAS density matrix in phase II exhibits a volume law

scaling of its logarithmic negativity, implying that it exhibits extensive long-range entanglement. We end this section by discussing the entropy production following a quench and by discussing the phase diagram for extensions of this model to higher dimensions or including a local bath. In Sec. IV we analyze the mutual information using a scattering state approach to the 3D non-interacting Anderson model and compare these results to a scattering state analysis of phase II in the random circuit. We find that the volume law mutual information in both models can be traced to the presence of “hidden” correlations between the scattering state wavefunctions. We present our conclusions in Sec. V. In Appendix A we present several general theorems that prove the existence of a set of NEAS density matrices for our random circuit model. In Appendix B we review some basic properties of the symmetric simple exclusion process (SSEP), which describes the time-averaged behavior of the random circuit model. In Appendix C we provide more details for the analysis of the scaling limit in phase II. In Appendix D we derive a compact representation of the replicated density matrix in the quantum chaotic phase. Finally, in Appendix E we present an analysis of the entanglement entropy of an open random circuit without charge conservation. For a zero entropy reservoir, we find that the entropy of the system is reduced by one bit, on average, compared to the infinite temperature state.

### III. LOCAL RANDOM CIRCUIT WITH CHARGE CONSERVATION

The random circuit model consists of a chain of  $L$  spin-1/2's or qubits, with additional spins at sites 0 and  $L+1$  that are coupled to the reservoirs. The only conserved quantity is the  $z$  component of the spin. The left/right reservoirs are taken to be in an infinite product state of mixed spin-1/2 states with magnetization  $m_{L/R}$  and no off-diagonal correlations or coherences. For the bulk dynamics we consider (described below), the time-averaged local magnetization in this system is linear in the position (see Fig. 1(b)). One of the primary motivating questions of this work is how close the NEASs (non-equilibrium attracting states) are to local equilibrium. Since there is only the one conserved quantity in our model, local equilibrium is defined as the maximal entropy mixed state that has the same average magnetization profile:

$$\rho_{\text{LE}} = \bigotimes_{i=1}^L \rho_{m_i}, \quad \rho_{m_i} = \left(\frac{1}{2} + m_i\right)u_i + \left(\frac{1}{2} - m_i\right)d_i, \quad (7)$$

$$m_i = m_L \left(1 - \frac{i}{L+1}\right) + m_R \frac{i}{L+1}, \quad (8)$$

where  $u_i = (1 + \sigma_z^{(i)})/2$  and  $d_i = (1 - \sigma_z^{(i)})/2$  denote projections of each site  $i$  onto spin up or down and  $m_{L/R}$  are the magnetizations of the left/right reservoir.

The dynamics are generated by a sequence of randomly chosen nearest-neighbor unitary operations, i.e., quan-

tum gates, applied at each time step, with no correlations between time steps (see Fig. 1(c)). After a gate operates on a boundary spin, that boundary spin is then immediately swapped with a “fresh” (uncorrelated) spin from the adjacent infinite reservoir. The unitary operations act on a given pair of neighboring sites (chosen with uniform probability at each time step) and, in the local basis  $|\uparrow\uparrow\rangle, |\uparrow\downarrow\rangle, |\downarrow\uparrow\rangle, |\downarrow\downarrow\rangle$ , take the form [56, 57]

$$U = \begin{pmatrix} U_+ & 0 & 0 & 0 \\ 0 & U_{ud} & U_{rl} & 0 \\ 0 & U_{lr} & U_{du} & 0 \\ 0 & 0 & 0 & U_- \end{pmatrix}. \quad (9)$$

The coefficients in  $U$  are chosen as follows: With probability  $p_1$  we apply a “non-interacting fermion” (NIF) gate defined by  $U_+ = U_-^* = e^{i\phi}$  with  $\phi$  a uniform random phase and the central  $2 \times 2$  matrix is a Haar random unitary on  $\text{SU}(2)$ . When acting only on nearest neighbors such a circuit can be efficiently simulated using a fermion representation of the qubits obtained by a Jordan-Wigner transformation [77]. In this case, the spin-density is mapped to the fermion density. These NIF gates are the only ones that perform a “partial swap,” where all four of  $U_{rl}, U_{lr}, U_{ud}, U_{du}$  are nonzero. With probability  $p_2 \leq (1 - p_1)$  we apply a randomly chosen unitary from one of two “interaction gate” sets that produce interactions between the fermions:

$$U_1 = e^{i\phi_1}u_1u_2 + e^{i\phi_2}u_1d_2 + e^{i\phi_3}d_1u_2 + d_1d_2, \quad (10)$$

$$U_2 = \text{SWAP} \cdot U_1, \quad (11)$$

where  $u_i$  and  $d_i$  are projectors onto up and down spins, respectively, the  $\phi_i$  are uniform random phases and SWAP exchanges the state of the two sites (SWAP is:  $U_+ = U_{rl} = U_{lr} = U_- = 1$  and  $U_{ud} = U_{du} = 0$ ). Note that these interaction gates do not perform partial swaps, which implies that states in the  $z$ -basis are mapped to a single-state in the  $z$ -basis. Finally, with probability  $1 - p_1 - p_2$  we apply either an iSWAP gate (SWAP with instead  $U_{lr} = U_{rl} = i$  so that it is in the NIF class) or the identity operation with equal probability. This last set of gates produce neither interactions nor partial swaps.

#### A. Time-averaged steady state

Although this system does not go to a time-independent steady state due to the noisy nature of the circuit, we provide three general theorems in Appendix A that can be used to prove an individual realization of this random circuit has a unique set of NEASs in the long-time limit. The ensemble of circuits, or the ensemble of all times for a single circuit produces a probability density  $\mathbb{P}(\rho)$  over the NEAS density matrices  $\rho$  that depends on the parameters  $p_1$  and  $p_2$ . The physical argument underlying the theorems is rather straightforward: Due to the diffusive transport in the system arising from swap and partial swap gates, after a time much greater than

$L^2$  ( $L + 1$  gates of the random circuit occur in one unit of time), the trajectory of each spin within the system must have involved a swap with a reservoir, which has no memory of the initial state within the system.

An important feature of this family of models is that the time averaged density matrix  $\bar{\rho} = \langle \rho(t) \rangle_t = \int d\rho \mathbb{P}(\rho) \rho$  is independent of  $p_1$  and  $p_2$ . Specifically, due to the random phases, the transport, and the swaps with the reservoirs, all off-diagonal terms in the density matrix average to zero such that

$$\bar{\rho} = \sum_{\{\tau_i\}} P(\tau_1, \dots, \tau_L) \bigotimes_{i=1}^L [\tau_i u_i + (1 - \tau_i) d_i], \quad (12)$$

where  $\tau_i \in \{0, 1\}$  is a pseudo-spin variable for site  $i$ . Averaging over random circuits we find that the probability measure  $P(\boldsymbol{\tau})$  has to satisfy the same steady state equation as a well-known classical, stochastic model of hard core particles, which goes under the name of the symmetric simple exclusion process (SSEP) [17]

$$\frac{dP(\boldsymbol{\tau})}{dt} = \sum_{\{\sigma_i\}} W_{\boldsymbol{\tau}}^{\boldsymbol{\sigma}} P(\boldsymbol{\sigma}) = 0. \quad (13)$$

We give the full expression for the transition matrix  $W_{\boldsymbol{\tau}}^{\boldsymbol{\sigma}}$  and review some basic properties of SSEP in Appendix B. This model is exactly solvable using a matrix product state (MPS) representation for  $P(\boldsymbol{\tau})$  with a bond dimension equal to  $L$  [78]. The diverging bond dimension in this model is needed to account for the long-range correlations induced by the currents. The average spin current between two sites satisfies an Ohm's law and is given by  $J_i = \langle \langle u_i - u_{i+1} \rangle \rangle_t = \delta / (L + 1)$ , where  $\delta = m_L - m_R$ ,  $\langle \cdot \rangle \equiv \text{Tr}[\rho \cdot]$ , and  $\langle \cdot \rangle_t$  denote time averages or, equivalently, averages over  $\mathbb{P}(\rho)$ .

## B. Phase diagram

The central results for the random circuit model can be summarized via the phase diagram shown in Fig. 2(a), while the key features of the bulk dynamics in the three phases are illustrated in Fig. 2(b-d). In Table I we list some of their defining characteristics. Since these three phases all have the same average  $\bar{\rho}$ , they can not be distinguished by any simple time-averaged measurements. But they do differ qualitatively in their  $\mathbb{P}(\rho)$ , which can be seen by the scaling of the instantaneous total entropy and mutual information of the NEAS. Alternatively, time-resolved measurements of two-point functions will generically distinguish these three phases.

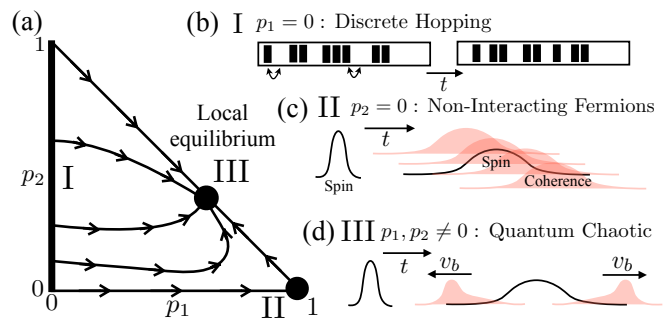


FIG. 2: (a) Phase diagram as a function of probabilities  $p_1$  and  $p_2$  determining the distribution of random unitaries in the random circuit. We find three distinct phases in the thermodynamic limit. Phase I is realized along the entire  $p_1 = 0$  axis. Phase II is realized for  $p_2 = 0$  and  $p_1 > 0$ . Turning on  $p_1 > 0$  always destabilizes phase I, as indicated by the schematic “flow lines.” Similarly, turning on  $p_2 > 0$  in phase II causes a “flow” to phase III. (b) Phase I has a mapping to a classical hard-core lattice gas with discrete hopping. (c) In Phase II both the spin and the coherences move and spread diffusively, (d) while in phase III the coherences spread ballistically at the butterfly speed  $v_B$ , rapidly reaching the boundaries where they are “decohered” by the reservoirs.

TABLE I: Properties defining the three phases. In phase III we can only bound the results for  $\Delta S$  and  $I(L : R)$  to second order in  $\delta$ .  $I(L : R)$  for  $\bar{\rho}$  is bounded by  $\log L$ .

	Transport	Operator Spreading	Entropy Production	$\Delta S$	$I(L : R)$
I	Diffusive/ Ohm's law	Diffusive	$\sqrt{t}$	Volume	0
II	"	Diffusive	$\sqrt{t}$	Volume	Volume
III	"	Ballistic	$t \rightarrow \sqrt{t}$	Area	Area

### 1. Phase I: Discrete hopping limit

For  $p_1 = 0$ , we can see by inspection that diagonal product states of the form

$$\rho_{\boldsymbol{\tau}} = \bigotimes_{i=1}^L [\tau_i \rho_{m_L} + (1 - \tau_i) \rho_{m_R}] \quad (14)$$

are attracting states of the random circuit, where  $\tau_i$  is a pseudo-spin variable that keeps track of whether a given density operator was originally inserted from the left or right reservoir. This is because the random phases for the gates in (10) do not affect this type of product state, while the SWAP's simply rearrange the configuration of on-site density matrices. If the initial state had any off-diagonal coherences in this  $u, d$  basis, these will diffuse to the boundaries and “disappear” in to the reservoirs. The dynamics within the NEAS manifold can then be mapped to SSEP where  $\rho_{m_L/m_R}$  maps to a pseudo-spin-up/down

state at a given site and the pseudo-spin reservoirs are fully polarized. This allows us to characterize the entire distribution function of the NEASs through the relation  $\mathbb{P}(\rho_\tau) = P(\tau)$  for  $P(\tau)$  satisfying (13) with  $\delta = 1$ . Note this is perhaps an unconventional perspective on classical SSEP, where we view the process as produced by one particular circuit, and for finite  $L$  for that specific circuit there is a unique time-dependent absorbing state  $\rho_\tau(t)$ .

We can find the average entropy of the NEASs by noting that

$$S(\rho_\tau) = N_L S(\rho_{m_L}) + N_R S(\rho_{m_R}), \quad (15)$$

where  $N_L$  is the total number of pseudo-spin-ups of the chain and  $N_R = L - N_L$  is the number of pseudo-spin-downs. Due to the pseudo-spin  $z$  inversion symmetry  $\langle N_L \rangle_t = \langle N_R \rangle_t = L/2$ . Considering the anti-symmetric case  $m_L = -m_R = \delta/2$  and comparing to local equilibrium, we find the volume law correction

$$\begin{aligned} \Delta S &\equiv S(\rho_{\text{LE}}) - \langle S(\rho) \rangle_t \\ &= L - L(1 - \delta^2) \tanh^{-1}(\delta)/\delta + O(L^0). \end{aligned} \quad (16)$$

In the limit  $\delta \rightarrow 1$ , the NEAS approaches a pure state and this deviation reaches its maximum possible value.

## 2. Phase II: Diffusive non-interacting fermions

For  $p_2 = 0$ , the NEASs have exact representations as Gaussian fermionic states because the dynamics are equivalent to that of non-interacting fermions and, in the fermion representation, the reservoirs are clearly Gaussian states. Such states are uniquely determined by their two-point function [79–81]

$$G_{ij} = \text{Tr}[\rho c_i^\dagger c_j], \quad (17)$$

$$S(\rho) = -\text{Tr}[(\mathbb{I} - G) \log(\mathbb{I} - G)] - \text{Tr}[G \log G], \quad (18)$$

where  $c_i$  are fermion annihilation operators related to the spin-lowering operator  $\sigma_-^{(i)}$  on each site via a Jordan-Wigner transformation. The operators  $c_i$  spread diffusively in this random circuit, leading to diffusive spreading of both the spin density  $n_i = c_i^\dagger c_i$  and the coherences  $c_i^\dagger c_j$  for  $i \neq j$  (see Fig. 2c). Again, any non-Gaussian features of the initial state will diffuse to the boundaries and disappear in to the reservoirs, leaving the Gaussian NEAS at long time. The presence of the log of the two-point function makes it difficult to compute the average entropy. For simplicity we restrict to anti-symmetric reservoirs  $m_L = -m_R = \delta/2$  and small  $\delta$  so that we can expand the log to find

$$\langle S(\rho) \rangle_t \approx -2 \text{Tr}[\bar{G} \log \bar{G}] - 2 \text{Tr}[\langle \delta G^2 \rangle_t], \quad (19)$$

where  $\bar{G} = \langle G \rangle_t$  and  $\delta G = G - \bar{G}$ . Since  $\bar{G}$  is just given by the linear magnetization profile, the first term is the

entropy of local equilibrium, while the second term accounts for the deviations arising from additional correlations and is determined by the covariance matrix

$$A_{ij} \equiv (1 - \delta_{ij}) \langle |c_i^\dagger c_j|^2 \rangle_t + \delta_{ij} (\langle n_i \rangle_t^2 - \langle n_i \rangle_t^2). \quad (20)$$

To solve for  $A_{ij}$ , we work in the scaling limit ( $L \rightarrow \infty$ ) for  $p_1 > 0$  and only compute the lowest order correction in a  $1/L$  expansion. Defining the coordinates  $x = i/L$  and  $y = j/L$ , we introduce the variables  $a(x, y) = A_{xL, yL+1}$  and  $b(x) = A_{xL, xL}$ . The restriction to nearest neighbor gates implies that, away from the diagonal  $x = y$ ,  $a(x, y)$  satisfies a diffusion equation with boundary conditions  $a(x, 1) = a(0, y) = 0$ . Integrating out the  $b(x)$  variable, one finds that  $a(x, y)$  has a constant source term along the diagonal given by  $-2J^2 L \delta(x - y) = -2\delta^2 \delta(x - y)/L$ . This diffusion problem has the solution (for  $x < y$ )

$$a(x, y) = \frac{x(1-y)}{L} \delta^2 + O(L^{-2}) + O(\delta^4). \quad (21)$$

The deviation from local equilibrium can be expressed perturbatively in  $\delta$  as

$$\Delta S \approx 4 \int_0^1 dy \int_0^y dx a(x, y) = \frac{\delta^2}{6} L. \quad (22)$$

which has a volume law correction away from both local equilibrium and the average entropy of phase I. We can also compute the mutual information of two sections of the chain cut at a point  $z \in (0, 1)$

$$\langle I(L : R) \rangle_t = \delta^2 z^2 (1 - z)^2 L + O(L^0) + O(\delta^4). \quad (23)$$

In sharp contrast to the  $p_1 = 0$  solution, we find that the NEASs have a volume law scaling of the mutual information, indicating that these states are highly correlated.

For mixed states, the mutual information is not a direct measure of entanglement as it can be dominated by classical correlations. In Sec. III C we explicitly show that the NEAS density matrix has volume law entanglement for sufficiently large  $\delta$  by computing a lower bound on the logarithmic negativity. When measured according to the fermionic logarithmic negativity recently introduced by Shapourian, Shiozaki, and Ryu [82], we find that this volume law scaling persists down to arbitrarily small  $\delta$ . This establishes that the NEAS density matrix is driven to a non-separable state in the large  $L$  limit. Thus, the volume law deviation of the entropy in phase II arises from entanglement and non-local correlations, while the deviation in phase I arises from “classical,” single-site magnetizations.

## 3. Phase III: Quantum chaotic

For nonzero values of  $p_1$  and  $p_2$ , the dynamics in the bulk are quantum chaotic as discussed in Sec. II A. Recall that the effective butterfly velocity  $v_B$ , which measures the speed of the ballistic operator front, scales as

$v_B^2 \sim \min(\sqrt{p_1 p_2}, p_2)$ , while the diffusion constant for conserved quantities is identical for all values of  $p_1$  and  $p_2$ . The calculation of the average entropy in this region is more difficult than in phases I and II because this random circuit does not map to an integrable model. To approach the calculation analytically, we instead work perturbatively in  $\delta$ . This allows us to expand  $\log \rho = \log(\bar{\rho} + \rho - \bar{\rho})$  to derive an expression for the average entropy similar to (19)

$$\Delta S \approx 2^{L-1} (\text{Tr}[\langle \rho^2 \rangle_t] - \text{Tr}[\bar{\rho}^2]), \quad (24)$$

which reduces the computation of the average entropy to the easier task of computing the average purity. The details of this calculation are described in Appendix D, while we give a brief summary here. The approach we take is to derive exact steady-state equations for the average replicated density matrix  $\langle \rho \otimes \rho \rangle_t$ . The solution to these equations can be mapped to the NESS of a fictitious six-species stochastic lattice gas model we refer to as the *abc*-model (Not to be confused with the *abc*-model introduced in Ref. [23]). We then use the ansatz that the  $n$ -point connected correlation functions of  $\langle \rho \otimes \rho \rangle_t$  have a scaling as  $\delta^n / L^{n-1}$  or smaller. This type of scaling is well known for SSEP and can be proved exactly for phase I and II. Using this ansatz, we find the lowest order correction to the entropy deviation from local equilibrium is given by

$$\Delta S = \frac{\alpha_1 \delta^2}{L p_1} + \frac{\alpha_2 \delta^2}{L p_2} + O(\delta^4) + O(L^{-2}), \quad (25)$$

where  $\alpha_{1/2}$  are constants independent of  $L$  and  $p_i$ . As a result, the average entropy is given by that of local equilibrium in the large  $L$  limit. This behavior is similar to SSEP, where the leading order  $L^0$  term in  $\Delta S$  at small  $\delta$  is  $\sim \delta^4$ . We can bound the higher order corrections to  $\Delta S$  since  $S(\rho_{\text{LE}}) \geq S(\bar{\rho}) \geq \langle S(\rho) \rangle_t$  and  $S(\bar{\rho})$  has been shown to be equal to  $S(\rho_{\text{LE}})$  up to a constant correction [18, 19]. To second order in  $\delta$ , we find the same scaling as (25) for the mutual information between two halves of the chain  $I(L : R)$ . Based on our analysis, we suspect that  $\mathbb{P}(\rho)$  is sharply peaked near  $\bar{\rho}$ , whose mutual information is bounded by  $\log L$  for large  $\delta$ , but further analysis is required to make more definitive statements about the mutual information at large values of  $\delta$  in this strongly interacting, quantum chaotic phase.

### C. Volume law entanglement in phase II

The von Neumann entropy and mutual information are not direct measures of entanglement for mixed state density matrices. Although a variety of entanglement measures for mixed states have been introduced [1], these measures are generally harder to compute than the von Neumann entropy because of the difficulty of distinguishing entanglement in many-body systems from non-local, classical correlations, which, for mixed states, can also

be generated by local operations and classical communication (LOCC) between the two regions. One efficiently computable measure of entanglement in the Hilbert space dimension is the logarithmic negativity  $\mathcal{E}(\rho)$ , which was originally introduced by Vidal and Werner [65].  $\mathcal{E}(\rho)$  has the property that, if it is non-zero, then the density matrix is non-separable (i.e., entangled) between the two regions. In bosonic or spin systems  $\mathcal{E}(\rho)$  is naturally defined using the partial transpose operation,

$$\langle i_A, j_B | \rho^{TA} | \ell_A, k_B \rangle \equiv \langle \ell_A, j_B | \rho | i_A, k_B \rangle, \quad (26)$$

where matrix elements are taken with respect to a separable orthonormal basis for regions  $A$  and  $B$ . The logarithmic negativity is

$$\mathcal{E}(\rho) \equiv \log \|\rho^{TA}\| \quad (27)$$

where  $\|A\| \equiv \text{Tr}[\sqrt{A^\dagger A}]$  is the trace norm.  $\mathcal{E}(\rho)$  is a measure of the strength and number of negative eigenvalues of  $\rho^{TA}$  and is an upper bound on the entanglement of distillation  $\mathcal{E}_D(\rho)$ .  $\mathcal{E}_D(\rho)$  is a more fundamental measure of entanglement defined as the maximum number of near-perfect singlet states that can be generated from multiple copies of  $\rho$  with LOCC on  $A$  and  $B$ . Although our underlying physical system in the random circuit model is a spin system, the logarithmic negativity for two adjacent regions in the original spin representation is equal to the logarithmic negativity of the fermions obtained after a Jordan-Wigner transformation [83]. Since we have an exact representation of the NEAS density matrix in phase II in terms of a Gaussian fermionic state, it is natural to ask whether we can directly compute the logarithmic negativity using this representation.

For fermionic systems a partial transpose operation can be defined analogously to (26); however, it has the property that the partial transpose of a fermionic Gaussian state may not be Gaussian, which makes the logarithmic negativity generally intractable to compute for large systems even for these simple fermionic states [83]. On the other hand, it was argued by Shapourian, Shiozaki, and Ryu that a more natural definition of the logarithmic negativity for fermions is in terms of a partial time reversal operation on sub-system  $A$  [82]. We refer to this measure as  $\mathcal{E}_f(\rho)$  to distinguish it from  $\mathcal{E}(\rho)$ . Unlike the partial transpose, this operation maps fermionic Gaussian states to fermionic Gaussian states, making it efficiently computable in the number of fermions. Although the precise significance of  $\mathcal{E}_f(\rho)$  as a measure of entanglement is not understood, for fermionic gaussian states it can be shown that it is an upper bound on the logarithmic negativity  $\mathcal{E}(\rho) \leq \mathcal{E}_f(\rho) + \log \sqrt{2}$  [83, 84]. Several efficiently computable lower bounds on  $\mathcal{E}(\rho)$  for Gaussian states were also introduced by Eisert, Eisler and Zimborás [84]. Here we use the lower bound  $\mathcal{E}_\ell(\rho)$  introduced by these authors for Gaussian states that conserve particle number:  $\text{Tr}[\rho c_i^\dagger c_j^\dagger] = \text{Tr}[\rho c_i c_j] = 0$  (see Sec. IV B of Ref. [84] for a definition of  $\mathcal{E}_\ell(\rho)$ ).

To compute the upper and lower bounds for the time averaged logarithmic negativity in phase II we use the



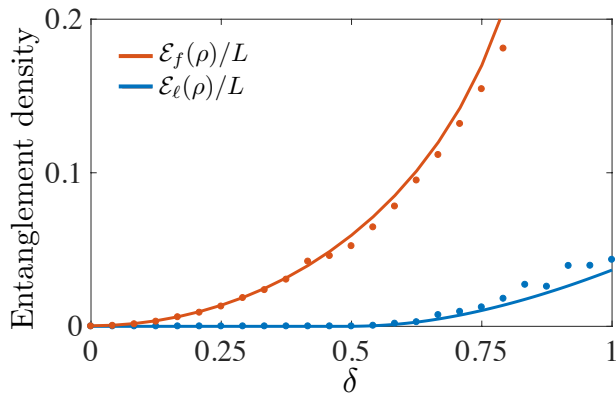


FIG. 3: Upper  $\mathcal{E}_f(\rho)$  and lower  $\mathcal{E}_\ell(\rho)$  bounds for the logarithmic negativity per unit length in phase II with  $p_1 = 1$  and  $p_2 = 0$ . The upper bound is equal to the fermionic logarithmic negativity [82]. Solid lines are for  $L = 10^3$  sites computed by randomly sampling the fermionic two-point function of the NEAS, which is valid for small  $\delta$ . Circles are computed from an exact simulation of the NEAS two-point function for the random circuit with  $L = 50$  sites. The volume law coefficient for  $\mathcal{E}_f(\rho)$  is non-zero for any  $\delta > 0$ , while the volume law coefficient of  $\mathcal{E}_\ell(\rho)$  is non-zero only for  $\delta > 0.5$ .

fact that all fourth and higher-order correlations of the matrix elements of the two-point function  $G_{ij}$  scale as  $\delta^4$  or higher. This allows us to sample random realizations of the NEAS two-point function by treating  $G_{ij}$  as independent, normally distributed random variables with mean  $\bar{G}_{ij}$  and variance  $A_{ij}$  (see Eq. (20)). Using this approach to sample from the NEAS, we are able to compute  $\mathcal{E}_{f,\ell}(\rho)$  for up to several thousand sites, which allows an accurate determination of the coefficient for the volume law term in  $\mathcal{E}_{f,\ell}(\rho)$  as a function of  $\delta$ . The results are shown in Fig. 3, where we compare this direct sampling approach for  $L = 10^3$  sites to exact simulations of the NEAS two-point function for realizations of the random circuit with  $p_1 = 1$ ,  $p_2 = 0$ , and  $L = 50$  sites. We find good agreement between the two independently computed coefficients up to  $\delta \approx 0.75$ . Interestingly,  $\mathcal{E}_f(\rho)$  exhibits volume law scaling for any finite  $\delta$ . On the other hand,  $\mathcal{E}_\ell(\rho)$  is exactly zero up until  $\delta = 0.5$ , at which point a clear volume law scaling emerges. The behavior of the lower bound proves definitively that the NEAS density matrix is non-separable in the scaling limit for  $\delta > 0.5$ . The sharp behavior of the lower bound suggests that the system may undergo a phase transition with increasing  $\delta$  from a separable to a non-separable state. However, we expect that the actual behavior of  $\mathcal{E}(\rho)$  is more like  $\mathcal{E}_f(\rho)$ , which exhibits a crossover to the volume law scaling for any finite  $\delta$ . Finally, we remark that it was recently proven that thermal mixed states of equilibrium spin models obey an area law for the logarithmic negativity [66]. Thus, similar to the observed volume law mutual information, this volume law scaling of  $\mathcal{E}(\rho)$  is a manifestly non-equilibrium effect.

## D. Entropy production following a quench

The discussion so far concerned average properties of each phase in the long-time limit. It is also interesting to consider the explicit time-dynamics of this model, where the effects of the ballistic operator spreading in the quantum chaotic region should be more manifest. Here we argue that, starting from an initial state that differs extensively in entropy from the NEAS, the ballistic operator spreading directly appears in the entropy production rate in the reservoirs following a quench into the chaotic phase.

For a quench in to phase I or II, all operators spread diffusively, implying that the system's net entropy change, which is only due to the reservoirs, will grow following the quench as  $\sim \sqrt{t}$  until it saturates on a time scale of order  $L^2$ . In contrast, in phase III any deviations from the NEAS can produce operators that spread ballistically to the boundary, so initially the increase in entropy can grow linearly in  $t$ . This fast entropy production will saturate on a timescale of order  $L/v_B$  as the system is brought to a local equilibrium. But if the magnetization profile in this initial local equilibrium is extensively away from the steady state then at later times diffusive spin transport is required for further entropy increase, leading to a crossover in time to diffusive relaxation of the local equilibrium state, which then finally approaches a NEAS by a time scale of order  $L^2$ .

## E. Extensions of the random circuit model

Two natural extensions of the random circuit model are to consider higher dimensional lattices with the left and right boundary of the lattice coupled to reservoirs or to allow each site to also be coupled to a qudit with local Hilbert space dimension  $q$ , which acts as a local bath for the qubit. The closed system dynamics for the qudit models were studied in Ref. [56, 57] by replacing  $U_+$  and  $U_-$  in the definition of the two-qubit unitaries in the bulk (see Eq. (9)) by two independent Haar random unitaries acting on the qudits. The central  $2 \times 2$  matrix was replaced by a Haar random unitary acting on the  $2q^2$  dimensional space spanned by  $|\uparrow\downarrow\rangle \otimes |nn'\rangle$  and  $|\downarrow\uparrow\rangle \otimes |nn'\rangle$ , where  $n$  and  $n'$  represent the state of the qudit on the two sites.

In the qudit model in arbitrary spatial dimensions, phase I still naturally appears by forbidding partial swaps of the state of the qubit. However, adding any finite probability  $p_1$  for partial swaps results in quantum chaotic dynamics even for  $p_2 = 0$ , which drives the system to local equilibrium (phase III, see Fig. 4). Effectively the qudits act as a quantum chaotic bath which can rapidly dissipate entropy into the reservoirs through ballistic operator spreading. For higher-dimensional lattices of qubits, phase I and phase III are naturally realized for  $p_1 = 0$  and any finite  $p_2$  and  $p_1$ , respectively. Furthermore, for  $p_2 = 0$  beyond 1D there is no longer a mapping of the

random circuit to a system of non-interacting fermions and the operator spreading becomes ballistic for any finite value of  $p_1$ . In this case, we expect that the system directly realizes phase III even along the  $p_2 = 0$  axis. The entanglement properties of the qudit models and the higher dimensional qubit models can be studied analytically using extensions of the *abc*-model discussed in Appendix D. Although we do not expect the higher dimensional random circuit models to naturally realize phase II, one can consider explicit non-interacting fermion models in higher dimensions to realize this phase, one example of which is discussed in Sec. IV.

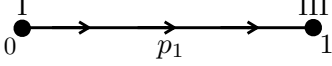


FIG. 4: Expected NEAS phase diagram as a function of the partial swap probability  $p_1$  for the random circuit model in higher spatial dimensions or with an additional qudit at each site in arbitrary dimensions [56, 57], which acts like a local bath for the qubit. Although phase I is preserved for  $p_1 = 0$ , there is no non-interacting fermion regime (phase II) in these models and we expect that the system immediately becomes quantum chaotic and achieves local equilibrium (phase III) for any finite  $p_1$ .

#### IV. NON-INTERACTING ANDERSON MODEL

The presence of the volume law mutual information in phase II arises from the diffusive spreading of the fermions produced by a Jordan-Wigner transformation of the spins. It is then natural to ask whether a similar effect occurs in a paradigmatic model for diffusive fermions: the Anderson model in 3D, with the Hamiltonian

$$H = t \sum_{\langle ij \rangle} c_i^\dagger c_j + \sum_i V_i c_i^\dagger c_i, \quad (28)$$

where  $t$  is the hopping, the first sum is over nearest-neighbor sites of a simple cubic lattice, and  $V_i$  is a random potential on each site. We draw  $V_i$  from a uniform distribution between  $\pm W/2$ . In 1D and 2D, any amount of disorder localizes the eigenstates, while in 3D this model has a metal-insulator transition near  $W_c/t \approx 16.3$  [85, 86]. We focus on the diffusive regime  $0 < W < W_c$ . Similar to the averaging over random unitaries in the circuit model, this model has characteristic disorder-averaged properties. For example, the disorder-averaged density-density response function in 3D at small  $(k, \omega)$  is simply dominated by a diffusive pole

$$\langle \chi(k, \omega) \rangle_d \sim \frac{4\pi\nu}{Dk^2 - i\omega}, \quad (29)$$

where  $D$  is the diffusion constant and  $\nu$  is the density of states, with the fluctuations of these diffusive modes well described by a nonlinear sigma model [87].

#### A. Entropy from scattering states

To determine the entanglement structure of the NESS for this Anderson model in contact with two reservoirs we use a description of the eigenstates of the system in terms of scattering states [69, 88, 89], as shown in Fig. 5. The leads are taken to be ballistic conductors with the same Hamiltonian as the disordered region, but with no random potential:  $V_i = 0$ . The incoming scattering states at a given energy  $E$  in transverse channel  $n$  are defined by a set of fermion operators  $a_\alpha^n(E)$  whose wavefunction satisfies the boundary condition that it is an incoming plane wave in lead  $\alpha$  and channel  $n$ . These operators have the correlation functions

$$\langle a_\alpha^{n\dagger}(E) a_\beta^m(E') \rangle = \delta(E - E') \delta_{\alpha\beta} \delta_{mn} \sigma_\alpha(E), \quad (30)$$

$$\sigma_\alpha(E) = \frac{1}{e^{(E - \mu_\alpha)/T} + 1}, \quad (31)$$

where  $\mu_\alpha$  is the chemical potential of lead  $\alpha$ , and  $T$  is the temperature which for simplicity we take to be the same in the two leads. The outgoing operators  $b_\alpha^n(E)$  are related to these incoming operators through the  $S$ -matrix.

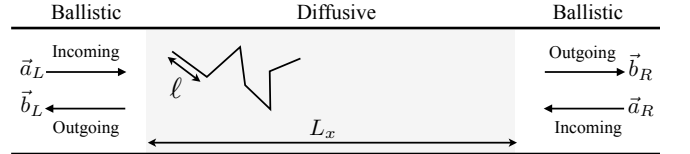


FIG. 5: Incoming and outgoing scattering states for a disordered wire with mean free-path  $\ell$ .

As in phase II, the reduced density matrix for the disordered region is entirely determined by the two-point function. Defining the wavefunction of the incoming scattering states

$$\phi_\alpha^n(\mathbf{r}, E) \equiv \langle \mathbf{r} | a_\alpha^n(E) | 0 \rangle, \quad (32)$$

the two-point function inside the wire is

$$\begin{aligned} \langle \psi^\dagger(\mathbf{x}) \psi(\mathbf{y}) \rangle &= \sum_n \int \nu dE [\delta\sigma(E) \phi_L^{n*}(\mathbf{x}, E) \phi_L^n(\mathbf{y}, E) \\ &+ \sigma_R(E) \sum_\alpha \phi_\alpha^{n*}(\mathbf{x}, E) \phi_\alpha^n(\mathbf{y}, E)], \end{aligned} \quad (33)$$

where  $\delta\sigma = \sigma_L(E) - \sigma_R(E)$  is the difference in the Fermi-functions of the two leads. The term proportional to  $\delta\sigma$  gives the non-equilibrium contribution to the two-point function. The excess fermion density in the wire due to the bias (assuming  $\delta\mu \equiv \mu_L - \mu_R > 0$ , and taking as our equilibrium reference the state when  $\mu = \mu_R$  in both leads) is given by

$$\delta n(\mathbf{x}) = \sum_n \int \nu dE \delta\sigma(E) |\phi_L^n(\mathbf{x}, E)|^2. \quad (34)$$

After disorder averaging,  $\langle \delta n(\mathbf{x}) \rangle_d$  will have the linear ramp profile discussed in Sec. II.

Similar to phase II, we can compute the corrections to the entropy by expanding the two-point function around its disorder average. The correction to the entropy of a given sub-region  $A$  will then be approximately equal to (see Eq. (19))

$$\Delta S_A \approx 2 \sum_{\mathbf{x}, \mathbf{y} \in A} \langle |\langle \psi_n^\dagger(\mathbf{x}) \psi_m(\mathbf{y}) \rangle|^2 \rangle_d - \langle n(\mathbf{x}) \rangle_d^2 \delta_{\mathbf{x}\mathbf{y}}, \quad (35)$$

which depends on the disordered average wavefunction correlations between different channels and energies. We parametrize these correlations by introducing the function

$$\begin{aligned} \Phi_A^{nm}(E, \Delta E) &= \sum_{\mathbf{x}, \mathbf{y} \in A} \langle \phi_L^{n*}(\mathbf{x}, E) \phi_L^m(\mathbf{x}, E + \Delta E) \\ &\times \phi_L^n(\mathbf{y}, E) \phi_L^{m*}(\mathbf{y}, E + \Delta E) \rangle_d \\ &- \sum_{\mathbf{x} \in A} \langle |\phi_L^n(\mathbf{x}, E)|^2 \rangle_d \langle |\phi_L^m(\mathbf{x}, E + \Delta E)|^2 \rangle_d. \end{aligned} \quad (36)$$

In the limit where  $\delta\mu, T \ll t \sim W$ , over the range of energies that contribute to the NESS,  $\Phi_A^{nm}(E, \Delta E)$  will only depend on the energy difference  $\Delta E$ . Taking the weakly-driven limit  $\delta\mu \ll T \ll t \sim W$  to compare to the random circuit, this allows us to approximate the entropy deviation from the disorder averaged reduced density matrix for region  $A$  as

$$\Delta S_A \approx \frac{2\nu^2 \delta\mu^2}{T} \sum_{nm} \int d\Delta E \Phi_A^{nm}(\mu_R, \Delta E). \quad (37)$$

The scaling of  $\Delta S_A$  with the geometry of  $A$  is determined by several factors. First, from the definition of the scattering states, the wavefunction amplitude scales as  $\phi_L^n(\mathbf{x}, E) \sim 1/L$ , where we have taken the two transverse linear dimensions of the leads and the diffusive region to be  $L$ . Assuming  $A$  is a finite fraction of the diffusive region, which is of length  $L_x$ , the sum over  $\mathbf{x}$  and  $\mathbf{y}$  involves on the order of  $L_x^2 L^4$  terms, which implies  $\Phi_A^{nm}(\mu_R, 0) \sim L_x^2$ . As we argued in Sec. II, the energy range over which the scattering state wavefunctions change on the length scale  $L_x$  is given by the Thouless energy  $E_{\text{Th}} \sim 1/L_x^2$ , which allows us to represent  $\Delta S$  as

$$\Delta S_A \approx \frac{2\nu^2 t \delta\mu^2}{T L_x^2} \sum_{nm} \Phi_A^{nm}(\mu_R, 0) \int d\epsilon s_A(\mu_R, \epsilon), \quad (38)$$

$$s_A(\mu_R, \epsilon) = \frac{\sum_{nm} \Phi_A^{nm}(\mu_R, \epsilon t L_x^{-2})}{\sum_{nm} \Phi_A^{nm}(\mu_R, 0)}, \quad (39)$$

where  $s(\mu_R, \epsilon)$  is independent of  $L_x$  in the scaling limit, but will depend on the aspect ratio  $L/L_x$  of the diffusive region. For diffusive wires in the regime  $L \ll L_x$ , the transmission through the wire satisfies the ‘‘isotropy’’ condition [90], which states that the wavefunctions in different transverse channels are completely uncorrelated at

each transverse slice of the wire. This assumption permits analytic treatments of the transmission and conductance through the wire using random matrix theory (RMT) [88]. For the scaling analysis of the entropy, this would imply that the sum over  $n$  and  $m$  can be reduced to a single sum over  $n$ , leading to an area law scaling with  $\Delta S_A$  independent of  $L_x$  in this  $L_x \gg L$  regime. However, in the regime  $L \sim L_x$ , this isotropy condition is known to break down [91], which allows additional correlations that violate the area law scaling.

Using numerical solutions of the scattering state wavefunctions based on the transfer matrix method [85, 86, 92, 93], we have confirmed that there is indeed a volume law scaling of the mutual information of two halves of the wire when the diffusive region has an aspect ratio of one. Our numerical results are summarized in Fig. 6. We consider a wire on a cubic lattice of size  $(L+2) \times L \times L$  with periodic boundary conditions in the transverse direction and strong disorder  $W/t = 8$ , but still well within the metallic phase ( $W_c/t \approx 16.3$ ). We parameterize the average mutual information between two regions as

$$\langle I(A : B) \rangle_d \approx \frac{\nu^2 t \delta\mu^2}{T} f_{AB}(\mu_R) L^2 \int d\epsilon i_{AB}(\mu_R, \epsilon), \quad (40)$$

$$i_{AB}(\mu_R, \epsilon) = \frac{\sum_{nm} \Delta \Phi_{AB}^{nm}(\mu_R, \epsilon t L_x^{-2})}{\sum_{nm} \Delta \Phi_{AB}^{nm}(\mu_R, 0)}, \quad (41)$$

$$\Delta \Phi_{AB}^{nm} = \Phi_{AB}^{nm} - \Phi_A^{nm} - \Phi_B^{nm}, \quad (42)$$

$$f_{AB}(\mu_R) = \frac{2}{L_x^2 L^2} \sum_{nm} \Delta \Phi_{AB}^{nm}(\mu_R, 0), \quad (43)$$

where  $i_{AB}(\mu_R, \epsilon)$  converges to a single function of  $\epsilon$  that is independent of  $L$  in the large  $L$  limit.

Taking  $A/B$  equal to the left/right half of the central  $L \times L \times L$  cube of the wire, Fig. 6(a) shows the scaling of  $|i_{AB}(\mu_R, \epsilon)|$  with  $L$ , demonstrating that it quickly converges to a universal curve. The converged function for  $i_{AB}(0, \epsilon)$  is well fit by a Gaussian decay  $e^{-\epsilon^2/2\sigma^2}$  at small values of  $\epsilon$  with  $\sigma \approx 5$ , but then changes sign and crosses over to a power law tail that is well fit by  $\epsilon^{-3/2}$  over this range of  $\epsilon$ . We note that a similar crossover at the Thouless energy to an  $\epsilon^{-d/2}$  tail has been observed in the spectral statistics of small metallic particles in dimension  $d$  [94]. For the parameters used in Fig. (6), we find that the integral of  $i_{AB}(0, \epsilon)$  over  $\epsilon$  is approximately equal to 4. The overall scaling of the mutual information with  $L$  is set by the term  $f_{AB}$ , which is shown in Fig 6(b). Fitting to  $f_{AB} = aL + b$ , we determine the coefficients

$$a \approx 0.021, \quad b \approx 0.038, \quad (44)$$

consistent with an overall volume law scaling for the mutual information. We leave a direct calculation of the logarithmic negativity  $\mathcal{E}(\rho)$  for future work. However, because of the similar structure of the fermionic two-point function of this model with phase II in the random circuit, we expect that the NESS will similarly exhibit a volume law scaling for entanglement.

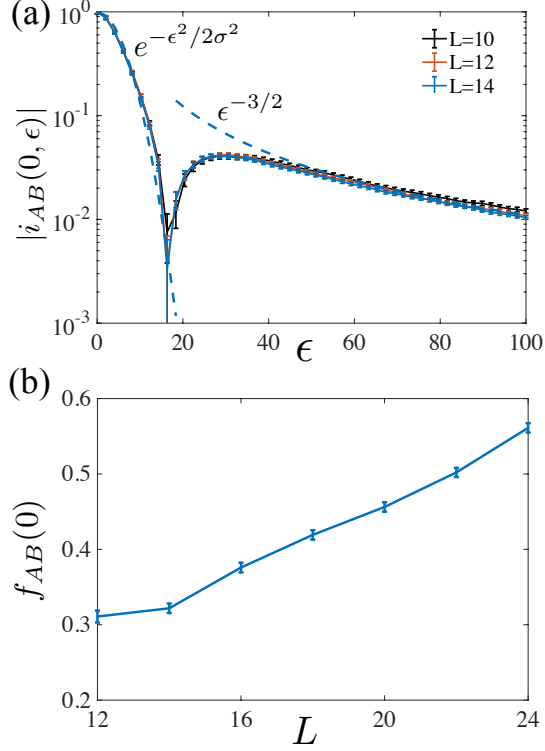


FIG. 6: (a) Energy correlation function  $|i_{AB}(0, \epsilon)|$  for the mutual information between two halves of the central  $L \times L \times L$  region of an  $(L+2) \times L \times L$  wire with  $t = 1$  and  $W = 8$  for 400 realizations of disorder. The approximate zero in the absolute value is due to a sign change. (b) Finite size scaling of  $f_{AB}$ , which determines the overall scaling of the mutual information. Parameters as in (a) with 1000 disorder realizations for each value of  $L$ . Error bars denote  $\pm 3$  standard deviations.

### B. Scattering state correlations in random circuit

In the case of the 3D Anderson model, we saw that the volume law mutual information arose from “hidden” correlations between different transverse channels of the scattering states. Here we show that a similar effect occurs in phase II of the random circuit model.

For the random circuit we do not have an identical notion of a scattering state as in extended Hamiltonian systems. Instead we define our scattering states to be the set of all reservoir operators at  $t = 0$ . Running the circuit forward in time, these reservoir operators will diffuse into and eventually out of the system on a time scale  $\sim L^2$ . At any instant of the circuit we thus have an over-complete set of operators given by the of order  $L^2$  reservoir operators that are still present and diffusing in the system. We can roughly understand the evolution of the probability amplitude of a single reservoir operator by coarse graining its evolution to a diffusion equation. In this case, it satisfies a standard diffusion equation with absorbing boundaries. Using the method of images, this diffusion

problem has the solution at early times

$$|\phi(x, t)|^2 \sim \frac{x}{t^{3/2} L^2} e^{-x^2/4Dt}, \quad t \ll 1 \quad (45)$$

where  $t = n/L^2$  and  $x = i/L$  are the rescaled discrete time  $n$  and space  $i$  variables, respectively. At late times, the dynamics are dominated by the slowest diffusive mode that satisfies the boundary condition that it vanishes at the edges

$$|\phi(x, t)|^2 \sim \frac{\sin \pi x}{L^2} e^{-\pi^2 D t}, \quad t \gg 1. \quad (46)$$

Thus, we see that the scattering states spread across the system on the diffusive time scale and have amplitude  $\sim 1/L$  before eventually leaking back out to the reservoirs.

Similar to Hamiltonian systems, we define an incoming scattering state wavefunction using the backward time evolution of the system operators

$$c_i^n = \sum_{\ell} \phi_{\ell}^i(n-m) c_{\ell}^m, \quad (47)$$

where  $c_{\ell}^m$  are the operators at time step  $m < n$  including both the system and the reservoir. Evolving sufficiently far backward in time that  $\phi_{\ell}^i(n-m)$  only has sizable overlap with the reservoir, we can express the two-point function in the system as

$$\langle c_i^{n\dagger} c_j^n \rangle = \sum_{\ell \in \text{Res}} \phi_{\ell}^{i*}(n-m) \phi_{\ell}^j(n-m) \langle c_{\ell}^{m\dagger} c_{\ell}^m \rangle, \quad (48)$$

where, similar to the Anderson model, we used the fact that scattering states in the reservoir are in an uncorrelated product state at negative times. For  $i = j$ , we see that (48) is a sum of order  $L^2$  terms with amplitude  $\sim 1/L^2$  and thus we find that the density in the system is always order one, as expected. For  $i \neq j$ , we can use the identity

$$\{c_i^{n\dagger}, c_j^n\} = 0 = \sum_{\ell \in \text{Res}} \phi_{\ell}^{i*}(n-m) \phi_{\ell}^j(n-m), \quad (49)$$

to rewrite the coherences for anti-symmetric reservoirs as

$$\langle c_i^{n\dagger} c_j^n \rangle = \delta \sum_{\ell \in \text{Left}} \phi_{\ell}^{i*}(n-m) \phi_{\ell}^j(n-m), \quad (50)$$

We immediately see that at equilibrium ( $\delta = 0$ ) the coherences vanish as expected. For finite  $\delta$ , we naively have a sum over  $L^2$  terms with random phases and amplitude  $1/L^2$ , which would result in the scaling

$$|\langle c_i^{n\dagger} c_j^n \rangle|^2 \sim \delta^2 / L^2. \quad (51)$$

Such a scaling would lead to an area law for the mutual information, in sharp contrast to what we found in Sec. IIIB. The resolution to this paradox is similar to the effect we found for the 3D Anderson model, where the volume law arose due to the presence of correlations between transverse channels. In the case of the random circuit, the volume law mutual information is recovered because of correlations between reservoir wavefunctions that persist over a finite time.

## V. CONCLUSION

While systems at thermodynamic equilibrium often satisfy area laws for their entanglement entropy or mutual information, any modification that drives the system out of equilibrium allows for potential violations of this behavior. In this paper we investigated a common non-equilibrium scenario consisting of an extended system coupled at its two ends to reservoirs at different chemical potentials, leading to current carrying non-equilibrium attracting states (NEASs) in the long-time limit. The analog of thermalization for these current-driven systems is the approach to local equilibrium. For a family of random circuit models, we found that the ballistic operator spreading associated with quantum chaos is crucial for the emergence of local equilibrium in these models. As our argument in favor of local equilibrium is rather general, it will be interesting to test these ideas in quantum chaotic Hamiltonian or Floquet driven systems. In addition, given that we found the mutual information of the NEASs in the quantum chaotic region is consistent with an area law, it is likely that these states can be well approximated using a matrix product representation, allowing a rich set of analytical and numerical techniques to be applied to further characterize these states.

A more surprising result is that, in one of the non-chaotic phases (phase II), we found that the system is driven towards a highly-entangled state with a volume-law mutual information and logarithmic negativity between two halves of the chain. This behavior demonstrates the ability to stabilize a high-degree of entanglement in non-equilibrium systems with limited fine-tuning of the evolution. For example, we showed that such extensive mutual information is also realized in the disordered 3D Anderson model for diffusive, non-interacting fermions, which is a widely used model for investigating transport. In the case of the Anderson model, we directly linked the volume law mutual information in the non-equilibrium steady state (NESS) to correlations between the scattering state wavefunctions in different scattering channels at a given energy. Future work could investigate the behavior of the NESS entanglement across the metal-insulator transition, where, naively, one expects a crossover to an area law scaling due to the localization of the wavefunctions. Using the mapping of disorder averaged Anderson models to supersymmetric field theories [87], it will be interesting to understand how the volume law mutual information of the NESS emerges in the corresponding field theoretic description. Determining more general conditions under which one can achieve such a strong violation of local equilibrium is a promising direction for future research. Finally, one is naturally led to ask whether such large deviations of the entropy away from local equilibrium or extensive entanglement can be harnessed as a thermodynamic resource or for applications in quantum information science.

In the context of open quantum systems, our work introduces the concept of NEAS density matrices to the

description of the long-time behavior of non-equilibrium open systems with noise or time-dependence in their parameters. In time-independent systems, there is a natural classification of NESSs into those described by low-entropy mixtures of a few pure states and high-entropy mixed states, with the latter often having an effective thermal description at long wavelengths [95]. Extending this classification program to the description of NEASs may prove a rich direction of research.

## Acknowledgments

*Acknowledgements.*—We would like to thank Vedika Khemani, Joel Lebowitz, Adam Nahum, Raghu Mahajan, Mike Zaletel, Brian Swingle, Marko Žnidarič, and Tomaž Prosen for helpful discussions and correspondence, and Arnold Mong for preliminary numerical work on a related Floquet system. Research supported by NSF DMR-1420541.

## Appendix A: Stationary random quantum circuits

In this appendix, we establish some basic facts about the long-time behavior of random quantum circuits coupled to reservoirs. This analysis demonstrates that the models considered in this paper have an attractive ensemble of density matrices in the long-time limit, which we refer to as non-equilibrium attracting states (NEASs).

For a given  $d$ -dimensional quantum system, an associated quantum channel  $\mathcal{E}(\cdot)$  is defined as a trace preserving, completely positive linear map that acts on the set of  $d \times d$  complex matrices  $M_d(\mathbb{C})$ . Every quantum channel has a representation in terms of a collection of Kraus operators  $\mathcal{E}_k$  satisfying  $\sum_r K_r^\dagger K_r = \mathbb{I}$  such that the density matrix of the system is transformed as [96]

$$\mathcal{E}(\rho) = \sum_r K_r \rho K_r^\dagger. \quad (\text{A1})$$

In this work we are interested in characterizing fixed points  $\mathcal{E}(\cdot)$ , defined as

$$\mathcal{F}_{ss}(\mathcal{E}) = \{\text{Density matrices } \rho_{ss} : \mathcal{E}(\rho_{ss}) = \rho_{ss}\}. \quad (\text{A2})$$

Since the set of density matrices is a compact, convex set in  $\mathbb{R}^n$  for  $n = d^2 - 1$ , Brouwer's fixed point theorem implies that every quantum channel has at least one fixed point. Some sufficient conditions for  $\rho_{ss}$  to be unique are described in Ref. [96].

We consider families of quantum channels  $\mathcal{E}_\sigma(\cdot)$  where  $\sigma$  is a random variable with probability measure  $d\sigma$  that takes on a possibly infinite set of values. If we introduce an additional measure  $d\nu$  on  $\mathcal{F}_{ss}(\mathcal{E}_\sigma)$  (e.g., determined by the distribution of initial states), this naturally induces a distribution of steady state density matrices  $\rho_{\sigma\nu}$  with measure  $d\sigma d\nu$ .

In the language of quantum channels, random circuits are defined as a sequence of independent random variables  $\sigma = (\sigma_1, \dots, \sigma_n)$  such that

$$\mathcal{M}_n(\rho) = \mathcal{E}_{\sigma_n} \circ \dots \circ \mathcal{E}_{\sigma_1}(\rho), \quad (\text{A3})$$

where the  $\mathcal{E}_{\sigma_i}$  are assumed to be drawn from identical distributions of random quantum channels. We focus on stationary random circuits defined by the property that  $\lim_{n \rightarrow \infty} \mathcal{M}_n(X) = \rho_\sigma \text{Tr}(X)$  with a probability that converges to one, where  $\rho_\sigma$  is a density matrix that is independent of the initial state  $X$  for all  $X \in M_d(\mathbb{C})$ . Such stationary random circuits have the convenient property that, for sufficiently large  $n$ ,  $\mathcal{M}_n(\cdot)$  induces a unique distribution of density matrices  $\rho_\nu$  with measure  $d\nu$ , which is stationary in the sense that  $\mathcal{E}_\sigma(\rho_\nu)$  is also distributed with measure  $d\nu$ . This property leads to the steady-state equations for the average replicated density matrices

$$\overline{\rho \otimes \dots \otimes \rho} = \int d\sigma \int d\nu \mathcal{E}_\sigma(\rho_\nu) \otimes \dots \otimes \mathcal{E}_\sigma(\rho_\nu). \quad (\text{A4})$$

For a given distribution of quantum channels  $\mathcal{E}_\sigma$ , the following two theorems are useful in determining whether the associated random circuit  $\mathcal{M}_n(\cdot)$  is stationary. First we prove that a wide class of random circuits are in fact stationary:

**Theorem A.1.** *Let  $\mathcal{M}_n(\cdot)$  be a random circuit that satisfies the following properties: (i) there exists  $m \in \mathbb{N}$  such that, with finite probability,  $\mathcal{M}_m(\cdot)$  has a one-dimensional set of fixed points and (ii)  $\mathcal{M}_n$  is almost surely diagonalizable for every  $n$ . Then  $\mathcal{M}_n(\cdot)$  is a stationary random circuit.*

*Proof.* Condition (i) implies that the quantum channel  $\mathcal{M}_n(\cdot)$  has a one-dimensional set of fixed points with a probability that converges to one with increasing  $n$ . For a given sequence  $\sigma$  of sufficiently large length, we denote the fixed point as  $\rho_\sigma$ . Condition (ii) implies that we can then almost surely represent  $\mathcal{M}_n(\cdot)$  as

$$\hat{\mathcal{M}}_n = P_\infty^\sigma + \sum_{k=1}^{d^2-1} \lambda_k^\sigma P_k^\sigma, \quad (\text{A5})$$

where  $\lambda_k^\sigma$  are the eigenvalues of  $\mathcal{M}_n(\cdot)$  with magnitude strictly less than one,  $P_k^\sigma$  are projectors into the eigenspaces,  $P_\infty^\sigma X = \rho_\sigma \text{Tr}(X)$  for all  $X \in M_d(\mathbb{C})$ , and  $P_\infty^\sigma + \sum_k P_k^\sigma = \mathbb{I}$ . Note that the second term in (A5) is always traceless when acting on  $X \in M_d(\mathbb{C})$  due to the fact that  $\mathcal{M}_n(\cdot)$  preserves the trace. This condition implies that

$$P_\infty^{\sigma'} \sum_k \lambda_k^\sigma P_k^\sigma = 0, \quad (\text{A6})$$

for all  $\sigma = (\sigma_1, \dots, \sigma_n)$  and  $\sigma' = (\sigma'_1, \dots, \sigma'_n)$ .

Now consider the limit as  $q \rightarrow \infty$  of the quantum channels

$$\hat{\mathcal{M}}_{qn} = P_\infty^{\mu_q} + \sum_k \lambda_k^{\mu_q} P_k^{\mu_q} P_\infty^{\mu_{q-1}} + \prod_{\ell=1}^q \sum_k \lambda_k^{\mu_\ell} P_k^{\mu_\ell}, \quad (\text{A7})$$

where  $\mu_\ell = (\sigma_{(\ell-1)n+1}, \dots, \sigma_{\ell n})$ . Denote by  $\lambda_{\max}^{\mu_\ell} = \max_k(|\lambda_k^{\mu_\ell}|)$  the maximum magnitude of the eigenvalues, now

$$\left\| \prod_{\ell=1}^q \sum_k \lambda_k^{\mu_\ell} P_k^{\mu_\ell} \right\|_\infty \leq \prod_{\ell=1}^q \left\| \sum_k \lambda_k^{\mu_\ell} P_k^{\mu_\ell} \right\|_\infty = \prod_{\ell=1}^q \lambda_{\max}^{\mu_\ell} \quad (\text{A8})$$

where  $\|A\|_\infty$  is the magnitude of the maximum eigenvalue of  $A$ . The RHS is a strictly decreasing sequence of positive real numbers, which must converge to zero as  $q \rightarrow \infty$ . Applying condition (ii) to  $\mathcal{M}_{qn}(\cdot)$  with  $\sigma = (\sigma_1, \dots, \sigma_{qn})$  results in the identities almost surely

$$P_\infty^\sigma = P_\infty^{\mu_q} + \sum_k \lambda_k^{\mu_q} P_k^{\mu_q} P_\infty^{\mu_{q-1}}, \quad (\text{A9})$$

$$\sum_k \lambda_k^\sigma P_k^\sigma = \prod_{\ell=1}^q \sum_k \lambda_k^{\mu_\ell} P_k^{\mu_\ell}. \quad (\text{A10})$$

Now, since the maximal eigenvalue  $\lambda_{\max}^\sigma$  converges to zero, this implies the convergence with probability one

$$\lim_{n \rightarrow \infty} \mathcal{M}_n(\rho) = \rho_\sigma, \quad (\text{A11})$$

□

The following theorem and a weakened version, both proved in Ref. [96], are helpful in determining whether a given  $\mathcal{M}_n$  satisfies condition (i) of Theorem A.1

**Theorem A.2.** *Let  $\mathcal{E} : M_d(\mathbb{C}) \rightarrow M_d(\mathbb{C})$  be a quantum channel with Kraus decomposition  $\mathcal{E}(\cdot) = \sum_i K_i \cdot K_i^\dagger$ . Denote by  $\mathcal{K}_m \equiv \text{Span}\{\prod_{k=1}^m K_{i_k}\}$  the complex linear span of all degree- $m$  monomials of Kraus operators forming  $\mathcal{E}_n(\cdot)$ . Then the following are equivalent: (1) For all density matrices  $\rho$  the limit  $\lim_{k \rightarrow \infty} \mathcal{E}^k(\rho)$  exists, is independent of  $\rho$  and given by a positive definite density matrix  $\rho_\infty$ . (2) There exists an  $m \in \mathbb{N}$  such that for all  $n \geq m$   $\mathcal{K}_n = M_d(\mathbb{C})$ .*

The modified version of this theorem has the weaker condition that we are only guaranteed the existence of an  $n \in \mathbb{N}$  such that  $\mathcal{K}_n = M_d(\mathbb{C})$ . In this case, the limit  $\lim_{k \rightarrow \infty} \mathcal{E}^k(\rho)$  exists, is independent of  $\rho$ , but is given by a positive semi-definite density matrix  $\rho_\infty$ . This version of the theorem applies to the restricted region of the phase diagram with  $p_1 = 0$ , where, for  $\delta = 1$ , the NEASs are given by pure states, i.e., rank one density matrices.

## Appendix B: The symmetric simple exclusion process

Here we review some basic properties of the symmetric simple exclusion process (SSEP) [17]. The transition matrix for SSEP can be decomposed into two single-site

boundary operators and  $L - 1$  two site operators in the bulk

$$W_{\tau}^{\sigma} = [R_L]_{\tau_1}^{\sigma_1} \otimes \mathbb{I} + [R_R]_{\tau_L}^{\sigma_L} \otimes \mathbb{I} + \sum_{i=1}^{L-1} [W_i]_{\tau_{i+1}}^{\sigma_{i+1}} \otimes \mathbb{I}, \quad (\text{B1})$$

where, in the local basis  $\{11, 01, 10, 00\}$ ,  $W_i$  is equal to an effective hopping matrix

$$W_i = \begin{pmatrix} 0 & 0 & 0 & 0 \\ 0 & -1/2 & 1/2 & 0 \\ 0 & 1/2 & -1/2 & 0 \\ 0 & 0 & 0 & 0 \end{pmatrix}, \quad (\text{B2})$$

while the boundary transition matrices for anti-symmetric reservoirs take the form

$$R_{L/R} = \frac{1}{4} \begin{pmatrix} -1 \pm \delta & 1 \pm \delta \\ 1 \mp \delta & -1 \mp \delta \end{pmatrix}. \quad (\text{B3})$$

This model has an exact solution in terms of a matrix product state (MPS) representation. Specifically,

$$P(\tau_1, \dots, \tau_L) = \langle U | A_{\tau_1} \cdots A_{\tau_L} | V \rangle, \quad (\text{B4})$$

where  $A_{L/R}$  are infinite dimensional matrices and  $|U, V\rangle$  are vectors that satisfy the algebraic equations

$$[A_L, A_R] = 2(A_L + A_R), \quad (\text{B5})$$

$$|V\rangle = \left( -\frac{1+\delta}{4} A_L + \frac{1-\delta}{4} A_R \right) |V\rangle, \quad (\text{B6})$$

$$\langle U| = \langle U| \left( -\frac{1+\delta}{4} A_R + \frac{1-\delta}{4} A_L \right). \quad (\text{B7})$$

From these relations it directly follows that (B4) satisfies Eq. (13). This algebra can be used to efficiently compute the probability amplitude of any configuration by recursively reducing the number of  $A_{\tau_i}$  matrices in the representation of  $P(\tau_1, \dots, \tau_L)$  from  $L$  to zero. Explicit representations of these matrices are given in Ref. [78]. The one, two and three point functions in the scaling

limit for  $x < y < z$  are given by [17]

$$\langle \tau_{Lx} \rangle = \frac{1+\delta}{2} - \delta x, \quad (\text{B8})$$

$$\langle \tau_{Lx} \tau_{Ly} \rangle = -\frac{x(1-y)}{L} \delta^2, \quad (\text{B9})$$

$$\langle \tau_{Lx} \tau_{Ly} \tau_{Lz} \rangle = -2 \frac{x(1-2y)(1-z)}{L^2} \delta^3. \quad (\text{B10})$$

### Appendix C: Scaling limit for phase II

In this appendix, we provide more details of the derivation of the volume law correction to the average entropy and mutual information for the non-interacting fermion random circuit. First, we note that the free-fermion gates acting on sites  $k$  and  $k+1$  obey the relation

$$U c_i^{\dagger} U^{\dagger} = \sum_j V_{ij} c_j^{\dagger} \quad (\text{C1})$$

where  $V_{ij}$  acts as the identity on most sites except when  $j$  is equal to  $k$  or  $k+1$ , in which case it is a Haar random matrix on  $U(2)$  with probability  $p_1$ , permutes sites  $k$  and  $k+1$  with probability  $(1-p_1)/2$  due to the action of the iSWAP, or is the identity with probability  $(1-p_1)/2$ . The action of the reservoir can also be simply accounted for by combining the action of the unitary gate, swap with the reservoir, and trace over the reservoir into a Kraus operator acting on the density matrix; however, in the scaling limit ( $L \rightarrow \infty$ ) a detailed consideration of the boundary operators is not necessary to lowest order in  $1/L$  as they only serve to set boundary conditions on the course-grained correlation functions.

The time-evolution equations for the components of the covariance matrix

$$A_{ij} \equiv \delta_{ij} (\bar{n}_i^2 - \bar{n}_i^2) + (1 - \delta_{ij}) |\overline{\langle c_i^{\dagger} c_j \rangle}|^2, \quad (\text{C2})$$

are given by

$$\overline{\langle c_{i_1}^{\dagger} c_{i_2} \rangle \langle c_{i_3}^{\dagger} c_{i_4} \rangle} (t + dt) = \sum_k \frac{1}{L} \int d\sigma \sum_{\{m_{\ell}\}} V_{i_1 m_1}^{k\sigma} V_{i_2 m_2}^{*k\sigma} V_{i_3 m_3}^{k\sigma} V_{i_4 m_4}^{*k\sigma} \overline{\langle c_{m_1}^{\dagger} c_{m_2} \rangle \langle c_{m_3}^{\dagger} c_{m_4} \rangle} (t), \quad (\text{C3})$$

where  $V_{ij}^{k\sigma}$  acts on sites  $k$  and  $k+1$  and  $d\sigma$  is the probability measure for the randomly chosen set of gates on that site. To compute this average we can use standard formulas for Haar averages of tensor products of matrices on  $U(n)$ . In particular, for a given  $k$  when  $i_{\ell}$  and  $m_{\ell}$  are all equal to either  $k$  or  $k+1$  we have the identity

$$\begin{aligned} \int d\sigma V_{i_1 m_1}^{k\sigma} V_{i_2 m_2}^{*k\sigma} V_{i_3 m_3}^{k\sigma} V_{i_4 m_4}^{*k\sigma} &= \frac{p_1}{3} \left[ \delta_{i_1 i_2} \delta_{i_3 i_4} \delta_{m_1 m_2} \delta_{m_3 m_4} + \delta_{i_1 i_4} \delta_{i_2 i_3} \delta_{m_1 m_4} \delta_{m_2 m_3} \right. \\ &\quad \left. - \frac{1}{2} \left( \delta_{i_1 i_4} \delta_{i_2 i_3} \delta_{m_1 m_2} \delta_{m_3 m_4} + \delta_{i_1 i_2} \delta_{i_3 i_4} \delta_{m_1 m_4} \delta_{m_2 m_3} \right) \right] \\ &\quad + \frac{1-p_1}{2} \left( \prod_{\ell=1}^4 \delta_{i_{\ell} m_{\ell}} + \prod_{\ell=1}^4 F_{i_{\ell} m_{\ell}}^{kk+1} \right), \end{aligned} \quad (\text{C4})$$

where  $F^{kk+1}$  is a permutation matrix for sites  $k$  and  $k+1$ . On the other hand, if only a pair of  $i_\ell$  indices are equal to  $k$  or  $k+1$  (e.g.,  $i_1$  and  $i_3$ ), we instead have the identity

$$\int d\sigma V_{i_1 m_1}^{k\sigma} V_{i_2 m_2}^{*k\sigma} V_{i_3 m_3}^{k\sigma} V_{i_4 m_4}^{*k\sigma} = \frac{1}{2} \left( \prod_{\ell=1}^4 \delta_{i_\ell m_\ell} + F_{i_1 m_1}^{kk+1} F_{i_3 m_3}^{kk+1} \delta_{i_2 m_2} \delta_{i_4 m_4} \right). \quad (\text{C5})$$

Using these relations, we find the equations of motion of the covariance matrix in the bulk  $2 \leq i \leq L-2$  and  $i+2 \leq j \leq L-1$

$$\begin{aligned} \frac{dA_{ii}}{dt} = & -\left(\frac{1}{2} + \frac{p_1}{6}\right) A_{ii} + \left(\frac{1}{4} - \frac{p_1}{12}\right) (A_{i-1i-1} + A_{i+1i+1}) + \frac{p_1}{3} (A_{ii+1} + A_{i-1i}) \\ & + \frac{\delta^2}{2(L+1)^2} - \frac{2i(L+1) - 2i^2 - 1}{6L(L+1)^2} \delta^2 p_1, \end{aligned} \quad (\text{C6})$$

$$\begin{aligned} \frac{dA_{ii+1}}{dt} = & -\left(\frac{1}{3} + \frac{2p_1}{9}\right) A_{ii+1} + \frac{p_1}{18} (A_{ii} + A_{i+1i+1}) + \frac{1}{6} (A_{i-1i+1} + A_{ii+2}) \\ & + \frac{2iL - 2i^2 + L}{18L(L+1)^2} \delta^2 p_1 \end{aligned} \quad (\text{C7})$$

$$\frac{dA_{ij}}{dt} = -\frac{1}{2} A_{ij} + \frac{1}{8} (A_{i-1j} + A_{i+1j} + A_{ij-1} + A_{ij+1}). \quad (\text{C8})$$

Before examining the steady-state solutions for finite  $p_1$ , it is constructive to examine their behavior for  $p_1 = 0$ , where we have an analytic solution for the distribution of NEASs. In this case, we see that  $A_{ii}$  decouples from  $A_{ii+1}$ , which becomes undriven. As a result,  $A_{ij} = 0$  for  $j \neq i$  and we are left with a discrete diffusion equation for  $A_{ii}$

$$A_{i-1i-1} - 2A_{ii} + A_{i+1i+1} = -\frac{2\delta^2}{(L+1)^2}. \quad (\text{C9})$$

We define  $b(x) = A_{xL, xL}$ , which, in the scaling limit, satisfies the boundary conditions  $b(0) = b(1) = 0$ , leading to the solution

$$b(x) = x(1-x)\delta^2 + O(L^{-1}). \quad (\text{C10})$$

An alternative derivation of this result is to use the mapping of  $\mathbb{P}(\rho_\tau)$  to SSEP with fully pseudo-spin polarized reservoirs to write

$$\overline{n_i^2} = \left(\frac{1+\delta}{2}\right)^2 \langle \tau_i \rangle + \left(\frac{1-\delta}{2}\right)^2 (1 - \langle \tau_i \rangle), \quad (\text{C11})$$

where  $\langle \tau_i \rangle = 1 - i/(L+1)$ , which agrees with (C10) in the scaling limit. Using this solution to compute the correction to the entropy we find

$$S(\rho_{\text{LE}}) - \langle S(\rho_\tau) \rangle_t = \frac{\delta^2}{3} L + O(L^0) + O(\delta^3), \quad (\text{C12})$$

which agrees with Eq. (16) expanded to order  $\delta^2$ .

For finite  $p_1$ , the solution to the steady-state exhibits crossover behavior in the scaling limit because the  $A_{ij}$  correlations are now sourced by the current along the diagonal. To solve for  $A_{ij}$ , we first invert the steady-

state solution of (C6) and find

$$\begin{aligned} A_{ii} = & \sqrt{\frac{p_1}{3}} \sum_j e^{-\lambda|i-j|} (A_{jj+1} + A_{j-1j}) \\ & + \frac{3(L+1) - 2i(L+1-i)p_1}{2L(L+1)^2 p_1} \delta^2, \end{aligned} \quad (\text{C13})$$

where  $\cosh \lambda = \frac{3+p_1}{3-p_1}$ . This expression is valid in the bulk up to exponentially small corrections on the order of  $e^{-\lambda L}$ . Notice that the second term is non-perturbative in  $p_1$ , which is consistent with the non-analytic behavior we find in the entropy and mutual information. Defining  $a(x, y) = A_{xL, yL+1}$ , we can rewrite the first term as

$$\begin{aligned} & \sqrt{\frac{p_1}{3}} \sum_j e^{-\lambda|i-j|} (A_{jj+1} + A_{j-1j}) \\ & \approx 4a(x, x) + \frac{3}{L^2 p_1} (\partial_x + \partial_y)^2 a(x, y)|_{x=y}. \end{aligned} \quad (\text{C14})$$

Inserting this identity into (C7) leads to the coarse-grained diffusion equation for  $a(x, y)$

$$\nabla^2 a = -\frac{2\delta(x-y)}{L} [\delta^2 + (\partial_x + \partial_y)^2 a]. \quad (\text{C15})$$

The second term on the RHS contributes an  $O(L^{-2})$  correction to  $a(x, y)$ , which is why we neglected it in the discussion in the main text.

#### Appendix D: Average replicated density matrix in chaotic phase III

In this appendix, we solve for the one and two point correlation functions of the time averaged replicated density matrix  $\langle \rho \otimes \rho \rangle_t$  perturbatively in  $\delta$  and  $L^{-1}$ . Using



the ansatz that the higher order connected correlation functions scale with higher powers of  $\delta$ , these correlation functions then allow us to compute the deviations of the average entropy and mutual information away from  $\bar{\rho}$ . As discussed in the main text, we find that the entropy converges to that of local equilibrium, while the mutual information obeys an area law to second order in  $\delta$ .

To describe the dynamics of the NEAS  $\rho_\nu$ , we first decompose the state into a complete set of orthogonal, Hermitian operators  $S$  normalized according to  $\text{Tr}(SS'^\dagger) = \delta_{SS'}$

$$\rho_\nu = \sum_S a_S^\nu S, \quad a_S^\nu = \text{Tr}(\rho_\nu S^\dagger). \quad (\text{D1})$$

The random channels that make up the random circuit map the state  $\rho_\nu$  to a different NEAS  $\mathcal{E}_\sigma(\rho_\nu)$ . Defining the coefficients  $e_{SS'}^\sigma$  by

$$\mathcal{E}_\sigma(S) = \sum_{S'} e_{SS'}^\sigma S', \quad (\text{D2})$$

the density matrix is updated as

$$\mathcal{E}_\sigma(\rho_\nu) = \sum_{SS'} e_{SS'}^\sigma a_{S'}^\nu S. \quad (\text{D3})$$

Then the average moments in the NEASs satisfy

$$\langle a_{S_1}^\nu \cdots a_{S_n}^\nu \rangle_t = \sum_{S'_i} \langle e_{S_1 S'_1}^\sigma \cdots e_{S_n S'_n}^\sigma \rangle_t \langle a_{S'_1}^\nu \cdots a_{S'_n}^\nu \rangle_t, \quad (\text{D4})$$

as a result the matrix  $\langle \rho^{\otimes n} \rangle_t$  is given by the NESS of a stochastic process in the space of operator strings with the transition matrix  $W_{SS'} = \langle e_{S_1 S'_1}^\sigma \cdots e_{S_n S'_n}^\sigma \rangle_t - \delta_{SS'}$  [54].

To compute the average entropy and mutual information to lowest order in  $\delta$  it is sufficient to have access to only the doubled matrix  $\langle \rho \otimes \rho \rangle_t$ . To solve for this

operator, we first reduce to a subset of the full Hilbert space that describes the NEASs. Unitarity of the bulk dynamics implies that  $\rho^2$  evolves with the same average dynamics as  $\rho$ . This implies that  $\langle \rho^2 \rangle_t$  has only diagonal components in the local  $z$ -basis, placing constraints on which second order moments  $\langle a_S a_{S'} \rangle_t$  are allowed to be non-zero. In particular, the only allowed operator string pairs  $(\begin{smallmatrix} S \\ S' \end{smallmatrix})$  at each site are one of the following six pairs

$$\left( \begin{smallmatrix} S \\ S' \end{smallmatrix} \right) = \left( \begin{smallmatrix} \dots \ell \dots r \dots u \dots d \dots u \dots d \dots \\ \dots r \dots \ell \dots u \dots d \dots d \dots u \dots \end{smallmatrix} \right), \quad (\text{D5})$$

where the single-site operators are taken as  $u = (1 + \sigma_z)/2$ ,  $d = (1 - \sigma_z)/2$ ,  $\ell = \sigma_-$ , and  $r = \sigma_+$ . This simplification reduces the size of the Hilbert space needed to represent  $\langle \rho \otimes \rho \rangle_t$  from  $16^L$  to  $6^L$ .

To describe the dynamics in this basis we make a formal mapping of each of these on-site operator pairs to one of three classes of spin-1/2 particles:  $a_\uparrow = \begin{pmatrix} \ell \\ r \end{pmatrix}$ ,  $a_\downarrow = \begin{pmatrix} r \\ \ell \end{pmatrix}$ ,  $b_\uparrow = \begin{pmatrix} u \\ d \end{pmatrix}$ ,  $b_\downarrow = \begin{pmatrix} d \\ u \end{pmatrix}$ ,  $c_\uparrow = \begin{pmatrix} u \\ d \end{pmatrix}$ , and  $c_\downarrow = \begin{pmatrix} d \\ u \end{pmatrix}$ . It is further convenient to make a Jordan-Wigner transformation on the  $\ell_i$  and  $r_i$  operators, which leads to an anti-commutation relation for the  $a$  and  $c$  particles. We can then map the solution for  $\langle \rho \otimes \rho \rangle_t$  to the NESS of a six species symmetric exclusion process in the space  $(\mu_1^{s_1}, \dots, \mu_N^{s_N})$ , where  $\mu_i \in \{a, b, c\}$ ,  $s_i \in \{\uparrow, \downarrow\}$ . We can evaluate the transition matrix in this representation following a similar approach as for the NIF random circuit making use of standard formulas for averages over Haar random unitaries. We find that the amplitude of each configuration  $P_L$  evolves according

$$\frac{dP_L(\mu^s)}{dt} = \sum_\sigma W_{\mu^s}^\sigma P_L(\sigma) \quad (\text{D6})$$

The two-site transition matrix in the bulk is a  $6 \times 6 \times 6 \times 6$  tensor with nonzero entries

$$W_0 = \begin{pmatrix} -\frac{1}{2} - \gamma_1 & \frac{1}{2} - \gamma_1 & \gamma_1 & \gamma_1 & \gamma_1 & \gamma_1 \\ \frac{1}{2} - \gamma_1 & -\frac{1}{2} - \gamma_1 & \gamma_1 & \gamma_1 & \gamma_1 & \gamma_1 \\ \gamma_1 & \gamma_1 & -\frac{1}{2} - \gamma_1 & \frac{1}{2} - \gamma_1 & -\gamma_1 & -\gamma_1 \\ \gamma_1 & \gamma_1 & \frac{1}{2} - \gamma_1 & -\frac{1}{2} - \gamma_1 & -\gamma_1 & -\gamma_1 \\ \gamma_1 & \gamma_1 & -\gamma_1 & -\gamma_1 & -\frac{1}{2} - \gamma_1 & \frac{1}{2} - \gamma_1 \\ \gamma_1 & \gamma_1 & -\gamma_1 & -\gamma_1 & \frac{1}{2} - \gamma_1 & -\frac{1}{2} - \gamma_1 \end{pmatrix}, \quad (\text{D7})$$

$$W_{a_s b_{s'}} = W_{b_s c_{s'}} = \begin{pmatrix} -\frac{1}{2} & \frac{1}{2} \\ \frac{1}{2} & -\frac{1}{2} \end{pmatrix}, \quad W_{a_s c_{s'}} = \begin{pmatrix} -\frac{1+\gamma_2}{2} & \frac{1-\gamma_2}{2} \\ \frac{1-\gamma_2}{2} & -\frac{1+\gamma_2}{2} \end{pmatrix}, \quad (\text{D8})$$

where  $\gamma_1 \equiv p_1/6$ ,  $\gamma_2 \equiv p_2$ ,  $W_0$  acts in the subspace  $\{b_\uparrow b_\downarrow, b_\downarrow b_\uparrow, c_\uparrow c_\downarrow, c_\downarrow c_\uparrow, a_\uparrow a_\downarrow, a_\downarrow a_\uparrow\}$  and  $W_{\mu_s \nu_{s'}}$  acts in the subspace  $\{\mu_s \nu_{s'}, \nu_{s'} \mu_s\}$ . The left boundary transition matrix is  $R_L = R_L^{bc} \oplus R_L^a$  where the matrix elements of  $R_L^{bc}$  in the basis

$\{b_\uparrow, b_\downarrow, c_\uparrow, c_\downarrow\}$  are

$$R_L^{bc} = \begin{pmatrix} -p_d^2(\frac{1}{2} - \gamma_1) - p_d p_u & p_u^2(\frac{1}{2} - \gamma_1) & \frac{p_u^2}{2} + \gamma_1 p_d p_u & \frac{p_u^2}{2} + \gamma_1 p_d p_u \\ p_d^2(\frac{1}{2} - \gamma_1) & -p_u^2(\frac{1}{2} - \gamma_1) - p_d p_u & \frac{p_d^2}{2} + \gamma_1 p_d p_u & \frac{p_d^2}{2} + \gamma_1 p_d p_u \\ \frac{p_d p_u}{2} + \gamma_1 p_d^2 & \gamma_1 p_u^2 + \frac{p_d p_u}{2} & -\frac{1}{2} + p_d p_u(1 - 2\gamma_1) & 0 \\ \frac{p_d p_u}{2} + \gamma_1 p_d^2 & \gamma_1 p_u^2 + \frac{p_d p_u}{2} & 0 & -\frac{1}{2} + p_d p_u(1 - 2\gamma_1) \end{pmatrix}, \quad (D9)$$

where  $p_u = (1 + \delta)/2$  and  $p_d = (1 - \delta)/2$ . The matrix elements of  $R_L^a$  in the basis  $\{a_\uparrow, a_\downarrow\}$  are

$$R_L^a = \begin{pmatrix} -1/2 & 0 \\ 0 & -1/2 \end{pmatrix}. \quad (D10)$$

The right boundary transition matrix  $R_R$  can be obtained by switching  $p_d$  and  $p_u$  in the expressions for  $R_L$ .

From these expressions we see the interacting gates effectively induce a dissipative interaction between  $a$  and  $c$  particles. This can be understood intuitively because the interactions effectively couple the off-diagonal correlations of the fermions to density-density fluctuations, which damp out the off-diagonal terms. Alternatively, the presence of these dissipative terms can be understood using the arguments given in the main text whereby the non-conserved operators spread ballistically to the reservoirs where they are decohered, which leads to a dissipation term in the bulk.

There are several helpful identities to keep in mind when working with this representation for  $\langle \rho \otimes \rho \rangle_t$ . First, the fact that  $\text{Tr}[\rho] = 1$  is reflected by the identity

$$1 = \langle \text{Tr}[\rho^2] \rangle_t = \sum_{\{\mu_i^{s_i} : \mu_i \in \{b, c\}\}} P_L(\mu_1^{s_1}, \dots, \mu_L^{s_L}). \quad (D11)$$

This conservation law is explicitly preserved by the bulk and boundary transition matrices. Similarly we can express the average purity as

$$\text{Tr}[\langle \rho^2 \rangle_t] = \sum_{\{\mu_i^{s_i} : \mu_i \in \{a, b\}\}} P_L(\mu_1^{s_1}, \dots, \mu_L^{s_L}). \quad (D12)$$

The average purity is preserved by the bulk transition matrices, which are associated with unitary dynamics; however, purity is not conserved by the boundary matrices. These boundary terms mix the  $b$  and  $c$  particles to preserve probability, but give rise to pure damping of the  $a$  particles. The reduced density matrices for a subset of sites  $A = \{i_1, \dots, i_n\} \subset \{1, \dots, L\}$  have the representation

$$\langle \rho^A \otimes \rho^A \rangle_t = \sum_{\{\mu_{i_j}^{s_{i_j}} : i_j \in A\}} P_A(\mu^s) \bigotimes_{j=1}^n \hat{\mu}_{i_j}^{s_{i_j}}, \quad (D13)$$

$$P_A(\mu_{i_1}^{s_{i_1}}, \dots, \mu_{i_n}^{s_{i_n}}) = \sum_{\{\mu_i^{s_i} : i \in A^c, \mu_i \in \{b, c\}\}} P_L(\mu^s), \quad (D14)$$

where  $A^c$  is the complement of  $A$ ,  $\rho^A = \text{Tr}_{A^c}[\rho]$ , and  $\hat{\mu}_i^{s_i}$  denotes the single-site operator in the doubled space corresponding to the label  $\mu_i^{s_i}$ .

In order to map the dynamics of  $P_L$  to a classical stochastic lattice gas, one requires that  $P_L \geq 0$  for all configurations of the particles. By definition, positivity of  $P_L$  is guaranteed for configurations that contain only  $a$  and  $b$  particles and only  $b$  and  $c$  particles; however, any configuration that contains a mixture of  $a$  and  $c$  particles is allowed to have negative weight. This fact should provide sufficient warning to the reader to avoid literally interpreting the dynamics of the  $abc$ -model as a classical stochastic lattice gas. On the other hand, for the problem at hand and sufficiently small values of  $\delta$ , we find that  $P_L$  does not have negative weight configurations in the large  $L$  limit. Thus our analysis provides an *a posteriori* justification for the interpretation of the  $abc$ -model as a classical stochastic lattice gas, but we do not assume the positivity of  $P_L$  in the analysis below.

To compute quantities such as the entropy, purity, or mutual information it is obviously sufficient to have access to arbitrarily high-order correlation functions. In the case of the NIF random circuit we took advantage of the fact that the NEASs are Gaussian fermionic states to represent the entropy in terms of two-point functions. For the full interacting problem such a simplification is no longer possible. Instead we take advantage of the fact that the only correlations in the system are perturbatively suppressed in the current  $J \sim \delta/L$ . This allows us to make an expansion of the NEAS density matrices around product states

$$\begin{aligned} \rho &= \bigotimes_{i=1}^L \rho_i + \sum_{\ell < m} \bigotimes_{i \neq \ell, m} \rho_i \otimes \delta \rho_{\ell m} \\ &+ \sum_{\ell < m < k} \bigotimes_{i \neq \ell, m, k} \rho_i \otimes \delta \rho_{\ell m k} + \dots, \end{aligned} \quad (D15)$$

where the  $\delta \rho_{\ell_1 \dots \ell_n}$  are defined recursively as the deviation of the reduced density matrix on sites  $\ell_1, \dots, \ell_n$  from the cluster expansion. This property implies that any partial trace over  $\delta \rho_{\ell_1 \dots \ell_n}$  is zero. Due to the fact that the NEASs for  $\delta = 0$  are product states, each of these terms must be at least order  $\delta$ .

To illustrate the validity of such an expansion for this class of current-driven problems we consider a few examples, focusing on the case of the NIF random circuit for  $p_2 = 0$ . For the NESS of SSEP represented as a density matrix, one can rigorously prove that these connected correlation functions satisfy the scaling [17]

$$\delta \rho_{\ell_1 \dots \ell_n} \sim \frac{\delta^n}{L^{n-1}} \quad (D16)$$

For the discrete hopping random circuit we saw that  $\delta\rho_{\ell_1\dots\ell_n} = 0$  for all  $n$ . In the case of the NIF random circuit, the mutual information between two halves of the chain satisfies a volume law, thus we know these states contain significant long-range correlations. Nevertheless, we will now argue that the expansion in (D15), which occurs in the original spin-basis instead of the fermionic basis, is still valid. In phase II we found that the off-diagonal matrix elements of  $\delta\rho_{\ell m}$  scale, with high-probability, as  $\delta/\sqrt{L}$ , while the diagonal elements scale as  $\delta^2/L^2$ . To evaluate the scaling of the higher-order connected correlation functions we can use the representation of  $\rho$  as a Gaussian fermionic state and Wick's theorem to relate these correlations to the two point functions. For example, the non-zero connected 3-point functions for  $i < j < k$  have the scaling for the off-diagonal correlations

$$\delta\langle r_i \ell_j u_k \rangle \equiv \langle r_i \ell_j u_k \rangle - \langle r_i \ell_j \rangle \langle u_k \rangle = -G_{ik} G_{kj} \sim \delta^2/L, \quad (\text{D17})$$

while the connected correlations on the diagonal scale as

$$\delta\langle u_i u_j u_k \rangle = 2\text{Re}[G_{ki} G_{ij} G_{jk}] \sim \delta^3/L^{3/2}. \quad (\text{D18})$$

More generally, we find that the off-diagonal connected correlation functions of length  $n$ , for  $n$  even, scale as  $\delta^{n/2}/L^{n/2}$ , while, for  $n$  odd, they scale as  $\delta^{(n+1)/2}/L^{(n+1)/2}$ . For the diagonal connected correlations we instead find the scaling  $\delta^n/L^{n/2}$ . Finally, we remark that an important feature of the class of NEASs we consider is that every density matrix in the ensemble has no correlations between states with different total  $z$ -angular momentum. This implies that the single-site density matrices  $\rho_i$  have no off-diagonal components. When evaluating the purity to order  $\delta^2$  we can represent

$$\begin{aligned} \text{Tr}[\rho^2] &= \text{Tr}\left[\left(\bigotimes_{i=1}^L \rho_i + \sum_{\ell < m} \bigotimes_{i \neq \ell, m} \rho_i \otimes \delta\rho_{\ell m}\right)^2\right] + O(\delta^3) \\ &= \prod_i \text{Tr}[\rho_i^2] + 2 \sum_{\ell < m} \prod_{i \neq \ell, m} \text{Tr}[\rho_i^2] \text{Tr}[\rho_\ell \rho_m \delta\rho_{\ell m}] \\ &\quad + \sum_{\ell < m} \prod_{i \neq \ell, m} \text{Tr}[\rho_i^2] \text{Tr}[\delta\rho_{\ell m}^2] + O(\delta^3). \end{aligned} \quad (\text{D19})$$

Here we were able to drop several terms because of the scaling

$$\text{Tr}[\rho_\ell \rho_m \delta\rho_{\ell m}] \text{Tr}[\rho_{\ell'} \rho_{m'} \delta\rho_{\ell' m'}] \sim \delta^4/L^4, \quad (\text{D20})$$

$$\text{Tr}[\rho_\ell \rho_m \rho_n \delta\rho_{\ell m n}] \sim \delta^3/L^{3/2}, \quad (\text{D21})$$

$$\text{Tr}[\rho_\ell \rho_m \rho_n \rho_k \delta\rho_{\ell m n k}] \sim \delta^4/L^2. \quad (\text{D22})$$

These scalings follow because multiplication by the single-site density matrices does not map off-diagonal terms of  $\delta\rho_{\ell_1\dots\ell_n}$  onto the diagonal, while the diagonal components have the scaling  $\delta\rho_{\ell m} \sim \delta^2/L^2$  and  $\delta\rho_{\ell m k} \sim \delta^3/L^{3/2}$ . Thus, despite the volume law mutual information in phase II, quantities such as the entropy

and mutual information can be computed with access only to non-extensive correlation functions of  $\rho$  and without knowledge of the Gaussian fermionic structure of the NEASs. The error in the  $n$ th order truncation scales as  $\delta^n$ .

For the quantum chaotic phase it is more convenient to apply the ansatz in (D15) to  $\langle \rho \otimes \rho \rangle_t$  instead of each instance of the random circuit. This is because the averaging over random circuits can induce correlations even between product state density matrices. For example, for  $p_1 = 0$  the NEASs are pure product states, while  $\mathbb{P}(\rho)$  encodes all the long-range correlations of the symmetric simple exclusion process (see Appendix B).

Based on (D12) and the symmetries of the problem for  $m_L = -m_R$ , to compute the average purity we need to find the correlation functions

$$\bar{b}_i^s \equiv P_{\{i\}}(b_i^s), \quad (\text{D23})$$

$$\delta b_{ij}^\uparrow \equiv P_{\{i,j\}}(b_i^\uparrow, b_j^\uparrow) - \bar{b}_i^\uparrow \bar{b}_j^\uparrow, \quad (\text{D24})$$

$$\delta b_{ij}^0 \equiv P_{\{i,j\}}(b_i^\uparrow, b_j^\downarrow) - \bar{b}_i^\uparrow \bar{b}_j^\downarrow, \quad (\text{D25})$$

$$a_{ij} \equiv P_{\{i,j\}}(a_i^\uparrow, a_j^\downarrow). \quad (\text{D26})$$

Expanding in  $\delta$  we note that the single-site correlation functions have to have the following structure

$$\bar{b}_i^\uparrow = \frac{1}{4} + \delta f_i + \delta^2 g_i + O(\delta^3), \quad (\text{D27})$$

$$\bar{b}_i^\downarrow = \frac{1}{4} - \delta f_i + \delta^2 g_i + O(\delta^3), \quad (\text{D28})$$

which follows because sending  $\delta \rightarrow -\delta$  should map  $\bar{b}_i^\uparrow \rightarrow \bar{b}_i^\downarrow$ . There is an additional constraint from conservation of probability that

$$2\bar{c}_i + \bar{b}_i^\uparrow + \bar{b}_i^\downarrow = 1, \quad (\text{D29})$$

where  $\bar{c}_i \equiv P_{\{i\}}(c_i^s)$  is independent of  $s$  by the definition of the  $c$ -particles. Making the ansatz that all the connected two-point functions are proportional to  $\delta^2$  we find that  $f_i$  satisfies the discrete diffusion equation in the bulk

$$f_{i-1} + 2f_i + f_{i+1} = 0. \quad (\text{D30})$$

Since  $\bar{b}_0^\uparrow = (1 + \delta)^2/4$  and  $\bar{b}_0^\downarrow = (1 - \delta)^2/4$ , this implies the solution

$$f_i = \frac{1}{2} - \frac{i}{L+1}. \quad (\text{D31})$$

To zeroth order in  $i/L$  we find  $g_i = f_i^2$ . To find the next order correction in  $1/L$  we define  $\delta g_i = g_i - f_i^2$ . Moving to the scaled coordinates  $x = i/L$  and  $y = j/L$ ,  $\delta g(x)$  satisfies the equation

$$\partial_x^2 \delta g = -2 + \frac{8\gamma_1 L^2}{1 - 2\gamma_1} \delta g_i + \frac{8\gamma_1 L^2}{\delta^2(1 - 2\gamma_1)} \delta J(x, x), \quad (\text{D32})$$

$$\delta J(x, y) = \delta b_{xLyL+1}^0 - \delta c_{xLyL+1}^0 - a_{xLyL+1}, \quad (\text{D33})$$

subject to the boundary condition  $\delta g(0) = \delta g(1) = 0$ . For constant  $\delta J(x, x)$ , except in an exponentially narrow region near the boundaries, this equation has the solution

$$\delta g = \frac{1 - 2\gamma_1}{4\gamma_1 L^2} - \frac{\delta J^2}{\delta^2}. \quad (\text{D34})$$

To determine the two-point functions we take advantage of the simplification that they are symmetric under the mapping  $\delta \rightarrow -\delta$ . This implies that the only unique two-point functions are:

$$\delta b_{ij}^\uparrow, \delta b_{ij}^0, \delta c_{ij}^\uparrow, \delta c_{ij}^0, \delta b c_{ij}, a_{ij} \quad (\text{D35})$$

where  $\delta b c_{ij} = P_{\{i,j\}}(b_i^s, c_j^{s'}) - \bar{b}_i^s c_j^{s'}$  for all  $s$  and  $s'$ . Furthermore, tracing over one of the sites gives the identities

$$\delta b c_{ij} = -\frac{1}{2}(\delta b_{ij}^\uparrow + \delta b_{ij}^0), \quad (\text{D36})$$

$$\delta b_{ij}^\uparrow + \delta b_{ij}^0 = \delta c_{ij}^\uparrow + \delta c_{ij}^0. \quad (\text{D37})$$

Using these identities and moving to scaled coordinates, we can derive diffusion equations for the  $b$ -correlations when  $x \neq y$

$$\nabla^2(\delta b^\uparrow + \delta b^0) = \frac{8\gamma_1 L^2}{1 - 2\gamma_1}(\delta b^\uparrow + \delta b^0), \quad (\text{D38})$$

$$\nabla^2(\delta b^\uparrow - \delta b^0) = 0. \quad (\text{D39})$$

These equations imply that the sum field is only non-zero in an exponentially narrow region near the diagonal  $x = y$ . Since this sum field is what enters in the evaluation of the trace, we have the result that it is primarily the diagonal components of the connected  $b$ -correlations that affect the purity. Evaluating these diagonal components we find that they scale as  $\delta^2/L^2$ , thus will give an order  $1/L$  correction to the purity and average entropy.

In the NIF random circuit, the volume law correction to the entropy arose from the  $a_{ij}$  field, which we found scales as  $\delta^2/L$ . For finite  $p_2$ , we find that  $a_{ij}$  has a similar source term  $\sim \delta^2/L^2$  as in the case of the NIF circuit; however, off the diagonal it rapidly decays at the rate  $\gamma_2$  due to the dissipation induced by the interactions. To lowest order in  $1/L$ , this leads to a similar diffusion equation for  $a(x, y)$  as (D38) with an exponential decay rate equal to  $\sqrt{\gamma_2}L$ . This implies that  $a(x, y)$  is only non-zero along the diagonal, where it scales as  $\delta^2/L^2$ . As a result, we find the average deviation of the entropy is given by

$$2^{L-1} \text{Tr}[\langle \rho^2 \rangle_t] = 2^{L-1} \text{Tr}[\bar{\rho}^2] + \frac{\alpha_1 \delta^2}{L p_1} + \frac{\alpha_2 \delta^2}{L p_2} + O(\delta^4) + O(L^{-2}), \quad (\text{D40})$$

where  $\alpha_{1/2}$  are constants, which we have not explicitly computed. Consequently, the average entropy and mutual information of the NEASs to lowest in  $1/L$  can be computed from  $\bar{\rho}$ . Thus the average entropy in the scaling limit converges to that of SSEP, where it is equal to local equilibrium up to a constant correction. Similarly, the mutual information obeys an area law up to this order in  $\delta^2$ .

## Appendix E: Open random quantum circuit without charge conservation

To compare to the random circuit with conservation laws studied in the main text, here we analyze an open random circuit without conservation laws acting on a spin chain with one end of the chain coupled to a zero entropy, spin-polarized reservoir. In this case we find that the NEASs have, on average, one bit of entropy less than the infinite temperature state. This result can be understood intuitively because as the reservoir becomes entangled with the system, it is also injecting known pure states. As shown in Fig. 7, this reduces the entropy of the system by one bit, which is spread non-locally across the entire chain due to the chaotic dynamics in the bulk.

The random circuit is composed of Haar random two-qubit unitaries  $U_{ii+1}^\mu$  acting on each pair of nearest neighbors. After a unitary is applied on site 0, this site is swapped with a spin from the reservoir. We can write the combined action of the unitary gate on sites 0 and 1 and the swap with the reservoir as a quantum channel acting on the reduced density matrix  $\rho$  for sites  $1, \dots, L$

$$\begin{aligned} \mathcal{E}_1^\mu(\rho) &= \text{Tr}_{R,0} \left[ U_{\text{swap}}^{R0} U_{01}^\mu \rho \otimes |\uparrow\uparrow\rangle\langle\uparrow\uparrow| U_{01}^{\mu\dagger} U_{\text{swap}}^{R0} \right] \\ &= \sum_r K_{1r}^\mu \rho K_{1r}^{\mu\dagger}, \end{aligned} \quad (\text{E1})$$

where  $U_{\text{swap}}^{R0}$  is a two-qubit swap operator acting on the reservoir and site 0. The two Kraus operators  $K_{1r}^\mu$  are given by the  $2 \times 2$  sub-matrices

$$U_{01}^\mu = \begin{pmatrix} K_{1\uparrow}^\mu & * \\ K_{1\downarrow}^\mu & * \end{pmatrix}, \quad (\text{E2})$$

where the basis is written as  $\{|\uparrow\uparrow\rangle, |\uparrow\downarrow\rangle, |\downarrow\uparrow\rangle, |\downarrow\downarrow\rangle\}$ . For the other sites, there is no interaction with the reservoir and

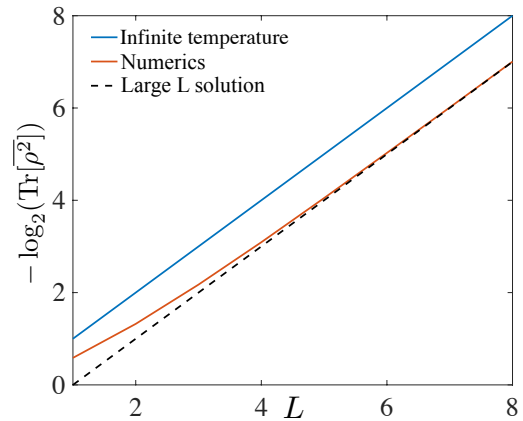


FIG. 7: Average purity of the NEASs for the open random circuit without charge conservation coupled to a zero temperature reservoir. The entropy is, on average, reduced by one bit compared to the infinite temperature state in the large  $L$  limit.

the quantum channels associated with each unitary have the representation  $\mathcal{E}_i^\mu(\rho) = U_{i-1i}^\mu \rho U_{i-1i}^{\mu\dagger}$ ,  $i = 2, \dots, L$ . Similar to the case analyzed in the main text, this random circuit evolves to a set of NEASs in the long time limit.

The time-averaged density matrix is simply given by the infinite temperature state  $\bar{\rho} = 2^{-L}\mathbb{I}$ ; however, since the reservoir has zero entropy we do not expect the higher order moments of  $\rho$  to be at infinite temperature. We can evaluate the average purity by noting that  $\bar{\rho}^2$  is also proportional to  $\mathbb{I}$ , which implies that the second order moments of the density matrix coefficients satisfy

$$\langle a_S a_{S'} \rangle_t \propto \delta_{SS'}. \quad (\text{E3})$$

For this problem we can then write the second order moment equations in the form

$$|a_S|^2 = \sum_{S'} W_{SS'} |a_{S'}|^2 \quad (\text{E4})$$

Further simplifications are possible by noting that, due to the symmetry of the problem, the average population of strings with  $S_i = X, Y, Z$  are equal in the NEASs. This allows us to represent each  $S \rightarrow 01001\dots$  by binary strings, where 0/1 denote whether a given site has a trivial/nontrivial operator [54]. In this case, the local Hilbert space for the strings is mapped to a pseudo-spin 1/2 and the update matrix takes the form

$$W = R \otimes \mathbb{I} + \sum_{i=1}^{L-1} W_i \otimes \mathbb{I}, \quad R = \begin{pmatrix} 0 & 0 \\ b & -d \end{pmatrix}, \quad (\text{E5})$$

$$W_i = \begin{pmatrix} 0 & 0 & 0 & 0 \\ 0 & -2/3 & 1/3 & 1/3 \\ 0 & 1/3 & -2/3 & 1/3 \\ 0 & 1/3 & 1/3 & -2/3 \end{pmatrix}, \quad (\text{E6})$$

where  $R$  acts on site 1 in the basis  $\{0, 1\}$  and  $W_i$  acts on sites  $i$  and  $i + 1$  in the basis  $\{00, 01, 10, 11\}$ . The birth and death rates of the non-trivial strings on site 1 are given by  $b = 0.2$  and  $d = 0.6$ , respectively.

The operator  $\bar{\rho}^2$  is fully determined by its trace

$$\bar{\rho}^2 = \frac{\mathbb{I}}{2^{2L}} \left( 1 + \sum_S |a_S|^2 \right). \quad (\text{E7})$$

Due to the mixing induced by the boundary, the populations  $p_1 = \sum_S |a_{1S}|^2$  and  $p_\mu = \sum_S |a_{\mu S}|^2$  have to be treated separately. We can write down a reduced Markov chain describing only the populations  $p_1 = \sum_S |a_{1S}|^2$ ,  $p_\mu = \sum_S |a_{\mu S}|^2$ , and the population in the identity string  $p_0$

$$\frac{d}{dt} \begin{pmatrix} p_0 \\ p_\mu \\ p_1 \end{pmatrix} = \begin{pmatrix} 0 & 0 & 0 \\ b & -d - \epsilon & b + \epsilon \\ 0 & \epsilon & -\epsilon \end{pmatrix} \begin{pmatrix} p_0 \\ p_\mu \\ p_1 \end{pmatrix}, \quad (\text{E8})$$

This Markov chain describes the process whereby the trivial string gives birth to a nontrivial operator at site 1. This operator then spreads throughout the system, leading to a finite mixing with  $p_1$  due to evolution under  $W_1$  at rate  $\epsilon \sim 1/3$ . The strings with a non-trivial operator at site 1 die at rate  $d$  and can be born from the non-trivial operator strings with the identity at site 1 at rate  $b$ . The steady state is independent of  $\epsilon$  and is given by

$$(p_0, p_\mu, p_1) = \left( 1, \frac{b}{d-b}, \frac{b}{d-b} \right) = (1, 1/2, 1/2). \quad (\text{E9})$$

The average purity is given by

$$-\log_2(\text{Tr}[\bar{\rho}^2]) = (L - 1), \quad (\text{E10})$$

which shows that the NEASs have, on average, one bit of entropy less than the infinite temperature state. We have checked that this analysis gives excellent agreement with numerics on small chains (see Fig. 7). There are small finite size corrections due to the fact that there is a slightly higher probability of the information bit being lost at site one, but these decay exponentially with  $L$ .

- 
- [1] R. Horodecki, P. Horodecki, M. Horodecki, and K. Horodecki, *Quantum entanglement*, Rev. Mod. Phys. **81**, 865 (2009).
  - [2] L. Bombelli, R. K. Koul, J. Lee, and R. D. Sorkin, *Quantum source of entropy for black holes*, Phys. Rev. D **34**, 373 (1986).
  - [3] M. Srednicki, *Entropy and area*, Phys. Rev. Lett. **71**, 666 (1993).
  - [4] M. M. Wolf, F. Verstraete, M. B. Hastings, and J. I. Cirac, *Area laws in quantum systems: Mutual information and correlations*, Phys. Rev. Lett. **100**, 070502 (2008).
  - [5] J. Eisert, M. Cramer, and M. B. Plenio, *Colloquium: Area laws for the entanglement entropy*, Rev. Mod. Phys. **82**, 277 (2010).
  - [6] J. M. Deutsch, *Quantum statistical mechanics in a closed system*, Phys. Rev. A **43**, 2046 (1991).
  - [7] M. Srednicki, *Chaos and quantum thermalization*, Phys. Rev. E **50**, 888 (1994).
  - [8] L. D'Alessio, Y. Kafri, A. Polkovnikov, and M. Rigol, *From quantum chaos and eigenstate thermalization to statistical mechanics and thermodynamics*, Adv. Phys. **65**, 239 (2016).
  - [9] S. R. White, *Density matrix formulation for quantum renormalization groups*, Phys. Rev. Lett. **69**, 2863 (1992).
  - [10] U. Schollwöck, *The density-matrix renormalization group*, Rev. Mod. Phys. **77**, 259 (2005).
  - [11] F. Verstraete, J. J. García-Ripoll, and J. I. Cirac, *Matrix product density operators: Simulation of finite-temperature and dissipative systems*, Phys. Rev. Lett. **93**,

- 207204 (2004).
- [12] K. Damle and S. Sachdev, *Nonzero-temperature transport near quantum critical points*, Phys. Rev. B **56**, 8714 (1997).
  - [13] D. T. Son and A. O. Starinets, *Hydrodynamics of R-charged black holes*, J. High Energ. Phys. **2006**, 052 (2006), arXiv:hep-th/0601157.
  - [14] C. P. Herzog, P. Kovtun, S. Sachdev, and D. T. Son, *Quantum critical transport, duality, and M theory*, Phys. Rev. D **75**, 085020 (2007).
  - [15] S. A. Hartnoll, P. K. Kovtun, M. Müller, and S. Sachdev, *Theory of the Nernst effect near quantum phase transitions in condensed matter and in dyonic black holes*, Phys. Rev. B **76**, 144502 (2007).
  - [16] C. Kipnis and C. Landim, *Scaling limits of interacting particle systems*, (Springer-Verlag Berlin, 1999).
  - [17] B. Derrida, *Non-equilibrium steady states: fluctuations and large deviations of the density and of the current*, J. Stat. Mech. **07**, P07023 (2007).
  - [18] C. Bahadoran, *On the convergence of entropy for stationary exclusion processes with open boundaries*, J. Stat. Phys. **126**, 1069 (2007).
  - [19] B. Derrida, J. L. Lebowitz, and E. R. Speer, *Entropy of Open Lattice Systems*, J. Stat. Phys. **126**, 1083 (2006).
  - [20] P. Gács, *Reliable computation with cellular automata*, J. Comput. Syst. Sci. **32**, 15 (1986).
  - [21] P. Gács, *Reliable Cellular Automata with Self-Organization*, J. Stat. Phys. **103**, 45 (2001).
  - [22] M. R. Evans, D. P. Foster, C. Godrèche, and D. Mukamel, *Spontaneous symmetry breaking in a one dimensional driven diffusive system*, Phys. Rev. Lett. **74**, 208 (1995).
  - [23] M. R. Evans, Y. Kafri, H. M. Koduvely, and D. Mukamel, *Phase separation in one-dimensional driven diffusive systems*, Phys. Rev. Lett. **80**, 425 (1998).
  - [24] R. A. Blythe and M. R. Evans, *Nonequilibrium steady states of matrix-product form: a solver's guide*, J. Phys. A: Math. Theor. **40**, R333 (2007).
  - [25] T. Prosen and M. Žnidarič, *Matrix product simulations of non-equilibrium steady states of quantum spin chains*, J. Stat. Mech. **2009**, P02035 (2009).
  - [26] T. Prosen, *Open XXZ Spin Chain: Nonequilibrium Steady State and a Strict Bound on Ballistic Transport*, Phys. Rev. Lett. **106**, 217206 (2011).
  - [27] T. Prosen, *Exact Nonequilibrium Steady State of a Strongly Driven Open XXZ Chain*, Phys. Rev. Lett. **107**, 137201 (2011).
  - [28] B. Buča and T. Prosen, *Exactly Solvable Counting Statistics in Open Weakly Coupled Interacting Spin Systems*, Phys. Rev. Lett. **112**, 067201 (2014).
  - [29] M. Žnidarič, *Anomalous nonequilibrium current fluctuations in the heisenberg model*, Phys. Rev. B **90**, 115156 (2014).
  - [30] C. Zanoci and B. G. Swingle, *Entanglement and thermalization in open fermion systems*, arXiv:1612.04840 (2016).
  - [31] F. Carollo, J. P. Garrahan, and I. Lesanovsky, *Current fluctuations in boundary-driven quantum spin chains*, arXiv:1802.00060 (2018).
  - [32] F. Heidrich-Meisner, A. Honecker, D. C. Cabra, and W. Brenig, *Zero-frequency transport properties of one-dimensional spin- $\frac{1}{2}$  systems*, Phys. Rev. B **68**, 134436 (2003).
  - [33] T. Prosen, *Chaos and complexity of quantum motion*, J. Phys. A: Math. Theor. **40**, 7881 (2007).
  - [34] Y. Huang, C. Karrasch, and J. E. Moore, *Scaling of electrical and thermal conductivities in an almost integrable chain*, Phys. Rev. B **88**, 115126 (2013).
  - [35] M. Žnidarič, *Exact solution for a diffusive nonequilibrium steady state of an open quantum chain*, J. Stat. Mech. **2010**, L05002 (2010).
  - [36] M. Žnidarič and M. Ljubotina, *Interaction instability of localization in quasiperiodic systems*, arXiv:1801.02955 (2018).
  - [37] K. Temme and F. Verstraete, *Stochastic Matrix Product States*, Phys. Rev. Lett. **104**, 210502 (2010).
  - [38] F. G. S. L. Brandao, T. S. Cubitt, A. Lucia, S. Michalakakis, and D. Pérez-García, *Area law for fixed points of rapidly mixing dissipative quantum systems*, J. Math. Phys. **56**, 102202 (2015).
  - [39] P. Hosur, X.-L. Qi, D. A. Roberts, and B. Yoshida, *Chaos in quantum channels*, J. High Energ. Phys. **2016**, 4 (2016), arXiv:1511.04021.
  - [40] R. Mahajan, C. D. Freeman, S. Mumford, N. Tubman, and B. Swingle, *Entanglement structure of non-equilibrium steady states*, arXiv:1608.05074 (2016).
  - [41] J. Haegeman and F. Verstraete, *Diagonalizing Transfer Matrices and Matrix Product Operators: A Medley of Exact and Computational Methods*, Annu. Rev. Condens. Matter Phys. **8**, 355 (2017).
  - [42] D. Ruelle, *Natural Nonequilibrium States in Quantum Statistical Mechanics*, J. of Stat. Phys. **98**, 57 (2000).
  - [43] Y. Ogata, *Nonequilibrium properties in the transverse XX chain*, Phys. Rev. E **66**, 016135 (2002).
  - [44] M. J. Bhaseen, B. Doyon, A. Lucas, and K. Schalm, *Energy flow in quantum critical systems far from equilibrium*, Nature Phys. **11**, 509 (2015).
  - [45] V. Eisler and Z. Zimborás, *Area-law violation for the mutual information in a nonequilibrium steady state*, Phys. Rev. A **89**, 032321 (2014).
  - [46] A. Coser, E. Tonni, and P. Calabrese, *Entanglement negativity after a global quantum quench*, J. Stat. Mech. **2014**, P12017 (2014).
  - [47] V. Eisler and Z. Zimborás, *Entanglement negativity in the harmonic chain out of equilibrium*, New J. Phys. **16**, 123020 (2014).
  - [48] M. Hoogeveen and B. Doyon, *Entanglement negativity and entropy in non-equilibrium conformal field theory*, Nucl. Phys. B **898**, 78 (2015).
  - [49] X. Wen, P.-Y. Chang, and S. Ryu, *Entanglement negativity after a local quantum quench in conformal field theories*, Phys. Rev. B **92**, 075109 (2015).
  - [50] P. Hayden and J. Preskill, *Black holes as mirrors: quantum information in random subsystems*, J. High Energ. Phys. **2007**, 120 (2007), arXiv:0708.4025.
  - [51] Y. Sekino and L. Susskind, *Fast scramblers*, J. High Energ. Phys. **2008**, 065 (2008), arXiv:0808.2096.
  - [52] N. Lashkari, D. Stanford, M. Hastings, T. Osborne, and P. Hayden, *Towards the fast scrambling conjecture*, J. High Energ. Phys. **2013**, 22 (2013), arXiv:1111.6580.
  - [53] A. Nahum, J. Ruhman, S. Vijay, and J. Haah, *Quantum entanglement growth under random unitary dynamics*, Phys. Rev. X **7**, 031016 (2017).
  - [54] A. Nahum, S. Vijay, and J. Haah, *Operator Spreading in Random Unitary Circuits*, arXiv:1705.08975 (2017).
  - [55] C. von Keyserlingk, T. Rakovszky, F. Pollmann, and S. Sondhi, *Operator hydrodynamics, OTOCs, and entanglement growth in systems without conservation laws*, arXiv:1705.08910 (2017).

- [56] V. Khemani, A. Vishwanath, and D. A. Huse, *Operator spreading and the emergence of dissipation in unitary dynamics with conservation laws*, arXiv:1710.09835 (2017).
- [57] T. Rakovszky, F. Pollmann, and C. W. von Keyserlingk, *Diffusive hydrodynamics of out-of-time-ordered correlators with charge conservation*, arXiv:1710.09827 (2017).
- [58] A. Chan, A. De Luca, and J. T. Chalker, *Solution of a minimal model for many-body quantum chaos*, arXiv:1712.06836 (2017).
- [59] A. Chan, A. De Luca, and J. T. Chalker, *Spectral statistics in spatially extended chaotic quantum many-body systems*, arXiv:1803.03841 (2018).
- [60] H. Gharibyan, M. Hanada, S. H. Shenker, and M. Tezuka, *Onset of Random Matrix Behavior in Scrambling Systems*, arXiv:1803.08050 (2018).
- [61] K. E. Nagaev, *On the shot noise in dirty metal contacts*, Phys. Lett. A **169**, 103 (1992).
- [62] K. E. Nagaev, *Influence of electron-electron scattering on shot noise in diffusive contacts*, Phys. Rev. B **52**, 4740 (1995).
- [63] V. I. Kozub and A. M. Rudin, *Shot noise in mesoscopic diffusive conductors in the limit of strong electron-electron scattering*, Phys. Rev. B **52**, 7853 (1995).
- [64] H. Pothier, S. Guéron, N. O. Birge, D. Esteve, and M. H. Devoret, *Energy Distribution Function of Quasiparticles in Mesoscopic Wires*, Phys. Rev. Lett. **79**, 3490 (1997).
- [65] G. Vidal and R. F. Werner, *Computable measure of entanglement*, Phys. Rev. A **65**, 032314 (2002).
- [66] N. E. Sherman, T. Devakul, M. B. Hastings, and R. R. P. Singh, *Nonzero-temperature entanglement negativity of quantum spin models: Area law, linked cluster expansions, and sudden death*, Phys. Rev. E **93**, 022128 (2016).
- [67] D. J. Thouless, *Electrons in disordered systems and the theory of localization*, Phys. Rep. **13**, 93 (1974).
- [68] P. W. Anderson, D. J. Thouless, E. Abrahams, and D. S. Fisher, *New method for a scaling theory of localization*, Phys. Rev. B **22**, 3519 (1980).
- [69] M. Büttiker, *Scattering theory of current and intensity noise correlations in conductors and wave guides*, Phys. Rev. B **46**, 12485 (1992).
- [70] C. W. J. Beenakker and M. Büttiker, *Suppression of shot noise in metallic diffusive conductors*, Phys. Rev. B **46**, 1889 (1992).
- [71] Y. M. Blanter and M. Büttiker, *Shot noise in mesoscopic conductors*, Phys. Rep. **336**, 1 (2000).
- [72] I. Klich and L. Levitov, *Quantum Noise as an Entanglement Meter*, Phys. Rev. Lett. **102**, 100502 (2009).
- [73] B. Hsu, E. Grosfeld, and E. Fradkin, *Quantum noise and entanglement generated by a local quantum quench*, Phys. Rev. B **80**, 235412 (2009).
- [74] G. Refael and J. E. Moore, *Entanglement entropy of random quantum critical points in one dimension*, Phys. Rev. Lett. **93**, 260602 (2004).
- [75] G. Refael and J. E. Moore, *Criticality and entanglement in random quantum systems*, J. Phys. A: Math. Theor. **42**, 504010 (2009).
- [76] X. Jia, A. R. Subramaniam, I. A. Gruzberg, and S. Chakravarty, *Entanglement entropy and multifractality at localization transitions*, Phys. Rev. B **77**, 014208 (2008).
- [77] B. M. Terhal and D. P. DiVincenzo, *Classical simulation of noninteracting-fermion quantum circuits*, Phys. Rev. A **65**, 032325 (2002).
- [78] B. Derrida, M. R. Evans, V. Hakim, and V. Pasquier, *Exact solution of a 1D asymmetric exclusion model using a matrix formulation*, J. Phys. A: Math. Gen. **26**, 1493 (1993).
- [79] M.-C. Chung and I. Peschel, *Density-matrix spectra of solvable fermionic systems*, Phys. Rev. B **64**, 064412 (2001).
- [80] S.-A. Cheong and C. L. Henley, *Many-body density matrices for free fermions*, Phys. Rev. B **69**, 075111 (2004).
- [81] I. Peschel and V. Eisler, *Reduced density matrices and entanglement entropy in free lattice models*, J. Phys. A: Math. Theor. **42**, 504003 (2009).
- [82] H. Shapourian, K. Shiozaki, and S. Ryu, *Partial time-reversal transformation and entanglement negativity in fermionic systems*, Phys. Rev. B **95**, 165101 (2017).
- [83] V. Eisler and Z. Zimborás, *On the partial transpose of fermionic Gaussian states*, New J. of Phys. **17**, 053048 (2015).
- [84] J. Eisert, V. Eisler, and Z. Zimborás, *Entanglement negativity bounds for fermionic Gaussian states*, arXiv:1611.08007 (2016).
- [85] A. MacKinnon and B. Kramer, *One-parameter scaling of localization length and conductance in disordered systems*, Phys. Rev. Lett. **47**, 1546 (1981).
- [86] J. L. Pichard and G. Sarma, *Finite size scaling approach to Anderson localisation*, J. Phys. C: Solid State Phys. **14**, L127 (1981).
- [87] K. Efetov, *Supersymmetry in Disorder and Chaos* (Cambridge University Press, Cambridge, UK, 1999).
- [88] C. W. J. Beenakker, *Random-matrix theory of quantum transport*, Rev. Mod. Phys. **69**, 731 (1997).
- [89] A. Bruch, C. Lewenkopf, and F. von Oppen, *Landauer-büttiker approach to strongly coupled quantum thermodynamics: Inside-outside duality of entropy evolution*, Phys. Rev. Lett. **120**, 107701 (2018).
- [90] P. A. Mello and A. D. Stone, *Maximum-entropy model for quantum-mechanical interference effects in metallic conductors*, Phys. Rev. B **44**, 3559 (1991).
- [91] R. A. Jalabert and J.-L. Pichard, *Quantum Mesoscopic Scattering: Disordered Systems and Dyson Circular Ensembles*, J. Phys. I France **5**, 287 (1995).
- [92] J. B. Pendry, A. MacKinnon, and P. J. Roberts, *Universality classes and fluctuations in disordered systems*, Proc. R. Soc. Lond. A **437**, 67 (1992).
- [93] K. Slevin and T. Ohtsuki, *Critical exponent for the Anderson transition in the three-dimensional orthogonal universality class*, New J. Phys. **16**, 015012 (2014).
- [94] R. A. Jalabert, J. L. Pichard, and C. W. J. Beenakker, *Long-Range Energy Level Interaction in Small Metallic Particles*, EPL **24**, 1 (1993).
- [95] L. M. Sieberer, M. Buchhold, and S. Diehl, *Keldysh field theory for driven open quantum systems*, Rep. Prog. Phys. **79**, 096001 (2016).
- [96] M. M. Wolf, *Quantum Channels and Operations: A Guided Tour*, lecture notes available at <http://www-m5.ma.tum.de/foswiki/pub/M5/Allgemeines/MichaelWolf/QChannelLecture.pdf> (2012).